

## Research article

## Resolving the role of podoplanin in the motility of papillary thyroid carcinoma-derived cells using RNA sequencing



Damian Mielecki<sup>a,\*</sup>, Ewa Gajda<sup>a,\*</sup>, Justyna Sikorska<sup>a</sup>, Anna Betkowska<sup>a</sup>,  
Marcin Rozwadowski<sup>a</sup>, Agata M. Gawel<sup>b</sup>, Maria Kulecka<sup>c</sup>, Natalia Zeber-Lubecka<sup>c</sup>,  
Marlena Godlewska<sup>a</sup>, Damian Gawel<sup>a</sup>

<sup>a</sup> Centre of Postgraduate Medical Education, Department of Cell Biology and Immunology, Marymoncka 99/103, 01-813 Warsaw, Poland

<sup>b</sup> Medical University of Warsaw, Histology and Embryology Students Science Association at the Department for Histology and Embryology, Chalubinskiego 5, 02-004 Warsaw, Poland

<sup>c</sup> Centre of Postgraduate Medical Education, Department of Gastroenterology, Hepatology and Clinical Oncology, Marymoncka 99/103, 01-813 Warsaw, Poland

## ARTICLE INFO

## Keywords:

ARHGAP  
ARHGEF  
BRAF V600E  
Metastasis  
Migration  
Papillary thyroid carcinoma  
Podoplanin  
RAC1  
RHOA  
Lamellipodia  
RNA sequencing

## ABSTRACT

The intracellular level of podoplanin (PDPN), a transmembrane protein of still unclear function, is frequently altered in metastatic tumors. High expression of PDPN is frequently observed in papillary thyroid cancer (PTC) specimens. Similarly, PTC-derived cell lines (BCPAP and TPC1, harboring the *BRAF* V600E mutation and *RET/PTC1* fusion, respectively), also present enhanced PDPN yield. We previously reported that depletion of PDPN impairs migration of TPC1 cells, but augments metastasis of BCPAP cells. Interestingly, this phenomenon stays in contrast to the migratory pattern observed for wild-type cells, where TPC1 exhibited higher motility than BCPAP cells. Here, we aimed to elucidate the potential role of PDPN in regulation of molecular mechanisms leading to the diverse metastatic features of the studied PTC-derived cells. We consider that this phenomenon may be caused by alternative regulation of signaling pathways due to the presence of the mutated *BRAF* allele or *RET/PTC1* fusion. The high-throughput RNA sequencing (RNA-seq) technique was used to uncover the genes and signaling pathways affected in wild-type and *PDPN*-depleted TPC1 and BCPAP cells. We found that changes in the expression of various factors of signaling pathways, like RHOA and RAC1 GTPases and their regulators, are linked with both high PDPN levels and presence of the *BRAF* V600E mutation. We imply that the suppressed motility of wild-type BCPAP cells results from overactivation of RHOA through natively high PDPN expression. This process is accompanied by inhibition of the PI3K kinase and consequently RAC1, due to overactivation of RAS-mediated signaling and the PTEN regulator.

## 1. Introduction

Podoplanin (PDPN) is a transmembrane, mucin-type protein encoded by the *PDPN* gene [1]. It is recognized as a lymphatic endothelial cell marker. PDPN consists of an external domain of ~130 amino acids (aa), a ~25 aa long transmembrane domain, and a short (~10 aa) intracellular tail and its reported molecular mass varies from 38 to 50 kDa [2,3]. The extracellular domain of PDPN is rich in serine and threonine residues with sialylated O-glycans [1]. The intracellular tail of PDPN interacts with the ezrin-radixin-moesin proteins (ERMs), protein kinase A (PKA) and cyclin-dependent kinase 5 (CDK5) [3,4]. It has also been reported that PDPN interplays with matrix metalloproteinase-14 and the cell surface receptor for hyaluronan, CD44 [5,6]. The only

currently known antigen that binds to the external domain is the C-type lectin-like receptor-2 (CLEC-2) located on the surface of platelets [5,7].

Importantly, various studies have linked PDPN with carcinogenesis. Altered expression of *PDPN* has been reported in numerous tumors, such as lung, ovarian and skin cancers, as well as glioblastoma [5,6]. PDPN has been shown to play a significant role in metastasis. Multiple *in vitro* studies have shown that *PDPN*-depleted cells exhibit decreased motility [8–10]. The interaction between PDPN and ERM family members, which triggers RHOA activation, was proposed as a potential mechanism of promotion of cellular epithelial-to-mesenchymal transition (EMT) and metastasis [1,5,11]. Furthermore, overexpression of *PDPN* has been found to lead to the suppression of immune cells allowing tumors to evade the anti-tumor immune response [5,12].

\* Corresponding authors.

E-mail addresses: [damian.mielecki@cmkp.edu.pl](mailto:damian.mielecki@cmkp.edu.pl) (D. Mielecki), [ewa.gajda@cmkp.edu.pl](mailto:ewa.gajda@cmkp.edu.pl) (E. Gajda).

<https://doi.org/10.1016/j.csbj.2023.07.035>

Received 18 April 2023; Received in revised form 14 July 2023; Accepted 25 July 2023

Available online 26 July 2023

2001-0370/© 2023 The Author(s). Published by Elsevier B.V. on behalf of Research Network of Computational and Structural Biotechnology. This is an open access article under the CC BY-NC-ND license (<http://creativecommons.org/licenses/by-nc-nd/4.0/>).

**Table 1**  
Primers used in the real-time RT-qPCR technique.

Gene name	Nucleotide sequences (5'→3')
<i>PDPN</i>	F: CGAAGATGATGTGGTGACTC R: CGATGCGAATGCCTGTTAC
<i>PTEN</i>	F: CAGAAGAAGCCCGCCAC R: TACGCCTTCAAGTCTTTCTCG
<i>PIK3CA</i>	F: GGGACCGATGCGGTTAG R: AAGTGGATGCCACAGTTTC
<i>DUSP5</i>	F: GTCCTCACCTCGCTACTC R: CATCCACGCAACTCAG
<i>DCP1A</i>	F: GTGTTATCCAGTGCCATC R: GCGTTCCAATAGTTAGAGG
<i>FRMD5</i>	F: ATCAAAGGGATCTCTACCATG R: ATCTCCGCTTGAAGGATGA
<i>PARP9</i>	F: GATATGCTTTGTAAAGTACAGGAGG R: AATAGTCCACTGCTAACGAG
<i>STAT3</i>	F: GGGTGGAGAAGGACATCAGCGGTAA R: GCCGACAATACTTTCCGAATGC
<i>PPP2CA</i>	F: CAAAAGAATCCAACGTGCAAGAG R: CGTTCACGGTAACGAACCTT
<i>SERPINE2</i>	F: AATGAAACCAGGATATGATTGAC R: TTGCAAGATATGAGAACATGGAG
<i>PIK3R1</i>	F: TGGACGGCGAAGTAAAGCATT R: AGTGTGACATTGAGGAGTGG
<i>18 S rRNA</i>	F: CCAGTAAGTGC GGTCATAAG R: CCATCCAATCGGTAGTAGCG

F, forward; R, reverse

**Table 2**  
Primary antibodies used in the study for Western blotting.

Antigen/ Catalog No.	Type/Clone (Symbol)	Dilution/ Blocking Agent	Source
β-actin/ 3700	Mouse monoclonal (IgG2b)/ 8H10D10	1:5000/ 5% skimmed milk	Cell Signaling Technology, Inc. (Beverly, MA, USA)
pAKT (S473)/ 4060	Rabbit monoclonal/ D9E	1:2000/ 5% BSA	Cell Signaling Technology, Inc.
tAKT/ sc-81434	Mouse monoclonal (IgG1)/ 5C10	1:500/ 5% skimmed milk	Santa Cruz Biotechnology, Inc. (Dallas, TX, USA)
CD44/ 3570	Mouse monoclonal (IgG2a)/ 156–3C11	1:2000/ 5% skimmed milk	Cell Signaling Technology, Inc.
pERK(T202/ Y204)/ 4370	Rabbit monoclonal/ D13.14.4E	1:2000/ 5% BSA	Cell Signaling Technology, Inc.
tERK/ 9102	Rabbit polyclonal	1:2000/ 5% BSA	Cell Signaling Technology, Inc.
pEZR (T567)/ ab47293	Rabbit polyclonal	1:1000/ 5% skimmed milk	Abcam (Cambridge, UK)
tEZR/ 3145	Rabbit polyclonal	1:2000/ 5% BSA	Cell Signaling Technology, Inc.
PDPN/ MCA2543	Mouse monoclonal (IgG1)/ D2–40	1:1000/ 5% skimmed milk	Bio-Rad Laboratories, Inc. (Hercules, CA, USA)
pSRC (Y416)/ 2101	Rabbit polyclonal	1:1000/ 5% BSA	Cell Signaling Technology, Inc.
tSRC/ 2110 S	Mouse monoclonal (IgG1)/ L4A1	1:1000/ 5% skimmed milk	Cell Signaling Technology, Inc.

In previous studies, we highlighted the association between *PDPN* expression and carcinogenesis by revealing high yield of *PDPN* in papillary thyroid carcinoma (PTC), the most commonly diagnosed subtype of thyroid cancer (TC). Interestingly, in normal thyroid tissue as

**Table 3**

Individual comparisons of selected samples of BCPAP and TPC1 cells, treated with negative control small interfering RNA (siRNA; siNEG) or *PDPN*-targeted siRNA (siPDPN).

	Comparison	Short name	Studied effect
(i)	BCPAP siNEG vs BCPAP siPDPN	B_N/ B_P	Effect of wild-type expression or knockdown of <i>PDPN</i> on the expression profile of the studied cells
(ii)	TPC1 siNEG vs TPC1 siPDPN	T_N/ T_P	
(iii)	BCPAP siNEG vs TPC1 siNEG	B_N/ T_N	Effect of presence/absence of the <i>BRAF</i> V600E mutation or <i>RET/PTC1</i>
(iv)	BCPAP siPDPN vs TPC1 siPDPN	B_P/T_P	rearrangement on the expression profile of the examined cells

well as in follicular thyroid cancer (FTC) and follicular adenoma (FA) specimens, *PDPN* expression was not detected [11,13]. A similar dependency was found in TC-derived cell lines, where *PDPN* was exclusively expressed in PTC-derived cells (BCPAP and TPC1) and not detected in FTC-derived FTC-133 cells [13].

Most importantly, previously performed studies on the role of *PDPN* in PTC indicated that TPC1 and BCPAP cells deficient in *PDPN* present an opposite motility pattern [11]. The migratory pattern observed in the controls (*PDPN*-expressing cells) showed decreased motility of BCPAP cells in comparison to TPC1 cells [11]. Interestingly, we found that *PDPN* depletion resulted in impaired migration and invasiveness of TPC1 cells, while *PDPN*-deficient BCPAP cells exhibited pro-metastatic activities [11]. Therefore, since the molecular basis of these observations remains unclear, we proposed that this phenomenon might be linked with *PDPN* expression and the genetic background of the studied cells, as BCPAP cells harbor the *BRAF* V600E allele and TPC1 contain the *RET/PTC1* rearrangement.

The *BRAF* V600E mutation is the most frequent genetic alteration in PTCs and is also often spotted in other tumors, including melanoma and colorectal cancers [14,15]. The *BRAF* gene encodes for the serine/threonine-protein kinase *BRAF*, which acts as a key regulator of the mitogen-activated protein kinase (MAPK) pathway. The presence of the *BRAF* V600E variant results in sustained activation of the MAPK signaling cascade, leading to enhanced proliferation, migration and survival of tumor cells [16–18]. On the other hand, TPC1 cells harbor the *RET/PTC1* fusion, which is another common alteration that occurs in PTC cells [19]. *RET* is a proto-oncogene encoding a receptor tyrosine-kinase that controls the proliferation and differentiation of cells [20]. The prevalence of the *BRAF* V600E mutation in PTCs reaches 83%, while the incidence of the *RET/PTC* rearrangement is estimated to be ~20% [21–23]. In most cases, these alterations are exclusive, but in less than 1% of all PTCs (older patients with advanced cancer), both mutations may appear [23]. Nevertheless, the clinical consequences of the presence of the *BRAF* V600E allele remain unclear. Some studies indicate poor prognosis for carriers of the *BRAF* mutation [24–26], while others show lack of correlation with overall survival and patients' condition [15,27,28]. The *RET/PTC1* rearrangement appears to be unrelated to any clinical features [20].

In the presented study we aimed to further elucidate the molecular background leading to the different metastatic features of the PTC-derived cells, BCPAP (*BRAF* V600E) and TPC1 (*RET/PTC1*), with knocked-down *PDPN*. Usage of the high-throughput RNA sequencing (RNA-seq) technique allowed us to reveal the molecular mechanisms underlying the opposite migratory potential phenomenon observed in *PDPN*-depleted BCPAP and TPC1 cells.

## 2. Materials and methods

### 2.1. Cell culture

Two model PTC-derived cell lines: BCPAP (harboring the *BRAF*

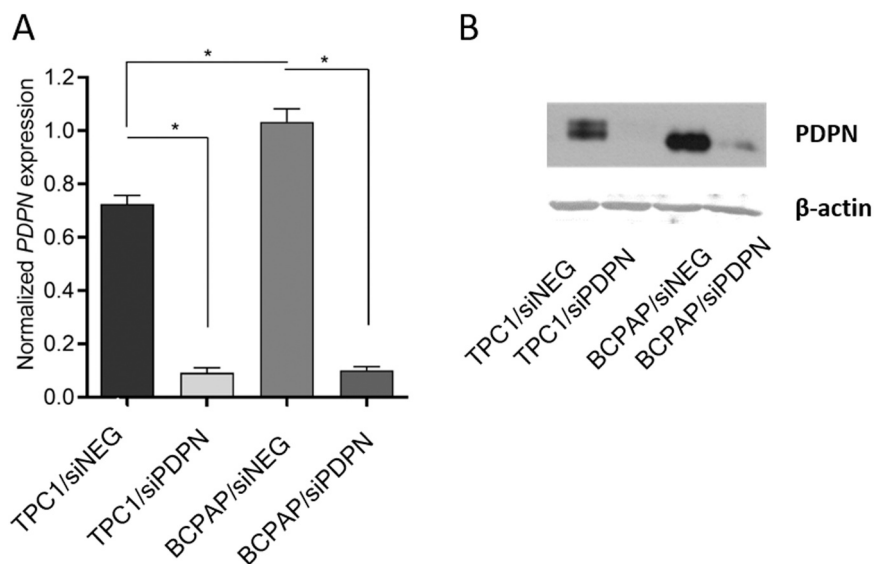


**Fig. 1.** Expression of podoplanin (PDPN) at transcript (A; RT-qPCR) and protein level (B; Western blot) in TPC1 and BCPAP cells transfected with PDPN-specific siRNA (siPDPN).  $\beta$ -actin served as a control in the Western blot analysis. Data are presented as mean  $\pm$  SD; \*  $p$ -value < 0.05.

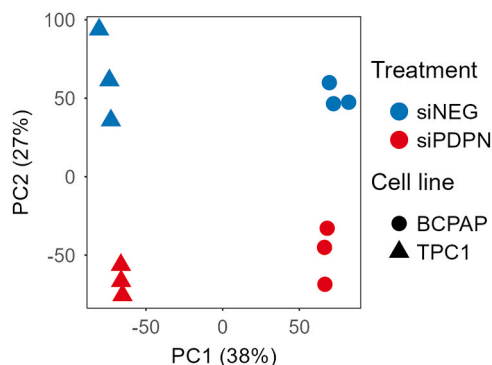


**Fig. 2.** Principal component analysis (PCA) of RNA-seq datasets calculated for TPC1 and BCPAP cells treated with negative control siRNA (siNEG) or siRNA targeting PDPN (siPDPN).

V600E mutation) and TPC1 (carrying the *RET/PTC1* rearrangement) were used in the study. The BCPAP cell line was purchased from the Leibniz Institute DSMZ-German Collection of Microorganisms and Cell Cultures GmbH, while the TPC1 cell line was originally provided by prof. M. Santoro (The University of Naples Federico II, Naples, Italy) and authenticated by short tandem repeat (STR) analysis at the American Type Culture Collection (ATCC). The cell lines were cultured in Roswell Park Memorial Institute (RPMI) 1640 medium supplemented with 10% fetal bovine serum (FBS; Corning, NY, USA) at 37 °C, in a humidified atmosphere containing 5% CO<sub>2</sub>.

## 2.2. Silencing of PDPN using small interfering RNA (siRNA)

Knockdown of *PDPN* expression in TPC1 and BCPAP cells was achieved using specific siRNA (siPDPN, siRNA ID: s20886, Silencer Select, ThermoFisher Scientific Inc., Rockford, IL, USA), which has previously been confirmed as highly effective [11,13]. MISSION siRNA Universal Negative Control (siNEG; Sigma-Aldrich, Steinheim, Germany) was used as a negative control. Cells were transfected with designated siRNA (30 nM) mixed with Lipofectamine 2000 (ThermoFisher Scientific Inc.) in Opti-MEM I Reduced Serum Medium (ThermoFisher Scientific Inc.), as described previously [11]. The efficacy of *PDPN* silencing was confirmed after 48 h or 72 h of incubation using real-time RT-qPCR and Western

blotting, respectively.

## 2.3. Total RNA isolation

Forty-eight hours after transfection, total RNA was isolated from cells using the GeneMATRIX Universal RNA Purification Kit (EURx, Gdansk, Poland) as described in the previous work [29]. Additionally, during RNA purification, the on-column DNase I (A&A Biotechnology, Gdynia, Poland) digestion was performed, according to the manufacturer's instructions. The purity and quantity of the isolated samples were assessed using a NanoDrop 2000/2000c spectrophotometer (ThermoFisher Scientific Inc.).

## 2.4. Reverse transcription and real time qPCR

For cDNA synthesis, 500 ng of purified RNA and a High-Capacity cDNA Reverse Transcription Kit with RNase Inhibitor (ThermoFisher Scientific Inc.) were used for the reaction (according to the manufacturer's protocol). Reverse transcription was followed by RT-qPCR to quantify the expression of the genes of interest. For real time qPCR, a mix composed of HOT FIREPol EvaGreen qPCR Mix Plus (Solis BioDyne, Tartu, Estonia), 2  $\mu$ L of 6-times diluted cDNA, and specific primers (0.5  $\mu$ M; listed in Table 1) was used. The reaction was performed in the CFX96 Detection System (Bio-Rad Laboratories, Inc., Hercules, CA, USA) with one cycle of 15 min at 95 °C and 40 cycles of 30 s at 95 °C, 60 s at 58 °C, 5 s at 65 °C. The expression of the target genes was calculated using the 2<sup>- $\Delta\Delta$ Ct</sup> method with 18S rRNA as a reference gene.

## 2.5. Western blotting

The cells were lysed 72 h after transfection, as previously described [29]. Briefly, the cells were washed 3-times with chilled phosphate-buffered saline (PBS, pH 7.3) and lysed on ice for 30 min using the RIPA Lysis and Extraction Buffer (ThermoFisher Scientific Inc.) supplemented with Pierce Phosphate Inhibitor Cocktail (ThermoFisher Scientific Inc.), Complete Protease Inhibitor Cocktail (Roche, Basel, Switzerland), and Viscolase (A&A Biotechnology). To assess the total protein concentration, the BCA Protein Assay Kit (ThermoFisher Scientific Inc.) was used. Protein lysates (20  $\mu$ g) were loaded into wells of a 9% SDS-PAGE gel and separated under reducing conditions. Next, electrophoretic transfer to a methanol-activated PVDF membrane (Merck, Burlington, MA, USA) was performed. Afterward, the

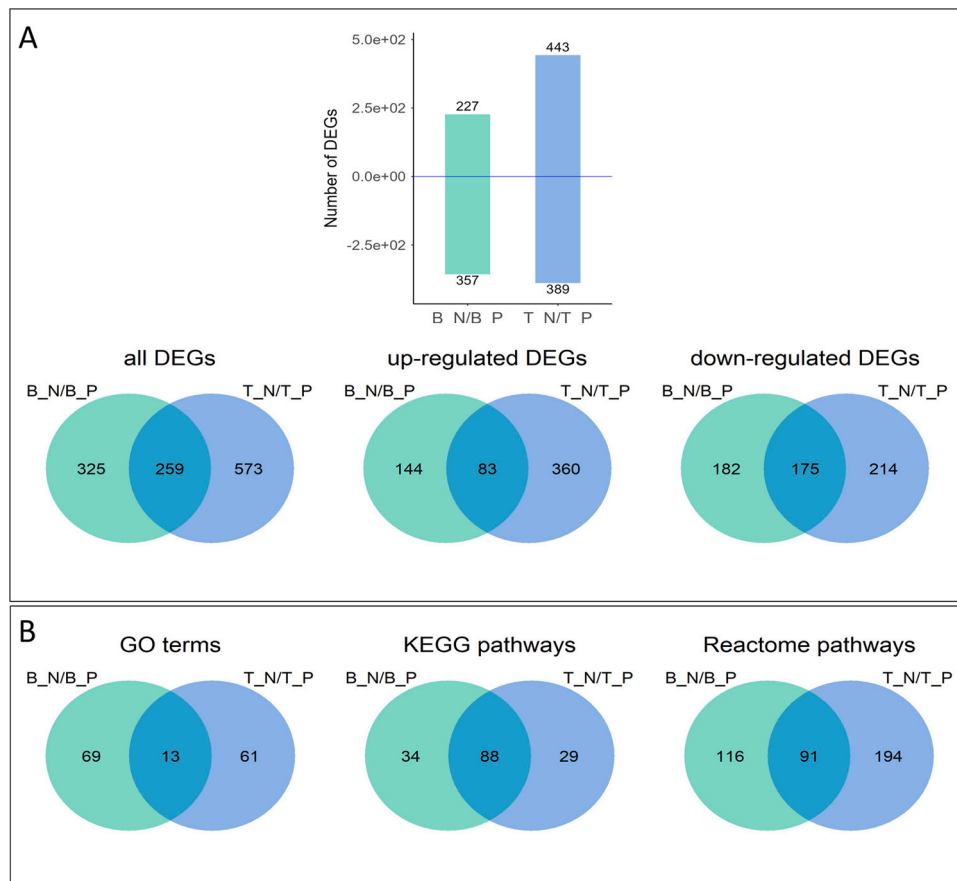


**Fig. 3.** A) The number of differentially expressed genes (DEGs): B\_N/B\_P (BCPAP siNEG vs BCPAP siPDPN) and T\_N/T\_P (TPC1 siNEG vs TPC1 siPDPN). B) The number of unique and common GO terms, KEGG, or Reactome pathways for comparisons showing the impact of PDPN expression, B\_N/B\_P and T\_N/T\_P. Only DEGs with  $|\log_2FC| \geq 1.5$  and adjusted  $p$ -value  $< 0.05$  were analyzed.

membrane was blocked with 5% skimmed milk in Tris-buffered saline containing 0.1% Tween 20 (TBST) at room temperature (RT) for 1 h, followed by overnight incubation (at 4 °C) with a primary antibody diluted in a dedicated blocking solution (Table 2). Subsequently, the membrane was extensively washed in TBST and incubated with a designated secondary antibody for 1 h at RT. The antibodies used in the study are listed in Table 2. After extensive washing in TBST, signals from the reactive bands on the membrane were detected using the Super-Signal West Dura Extended Duration Substrate (ThermoFisher Scientific Inc.). The densitometry analysis of Western blot data was performed in ImageJ 1.53 t [30]. The measurement results of active form(s) (phosphorylated) were normalized against the total yield of the corresponding protein (of  $\beta$ -actin in the case of CD44), according to the following equation:  $D_R = (D_A/D_T) \times 100$ , where:  $D_R$  – relative densitometry;  $D_A$  – densitometry of the band of active form;  $D_T$  – densitometry of the band of total form.

## 2.6. RNA sequencing (RNA-seq) library preparation

The quantity, purity, and integrity of the extracted RNA fractions (RNA integrity number, RIN) were measured using the Agilent RNA 6000 Nano Kit (Agilent Technologies, Inc., Santa Clara, CA, USA) and 2100 Bioanalyzer (Agilent Technologies, Inc.). Only samples with RIN values of 8 or greater were used for construction of the cDNA libraries. For each sample, total RNA (100 ng) was assessed with the Qubit RNA HS Assay Kit (ThermoFisher Scientific Inc.) and used for construction of libraries with the Ion AmpliSeq Transcriptome Human Gene Expression Panel (ThermoFisher Scientific Inc.), according to the manufacturer's protocol. Next, reverse transcription of RNA, subsequent cDNA

purification, and libraries size selection were performed. Constructs were then analyzed for sample quality control, yield, and size distribution using the Agilent 2100 Bioanalyzer system and a High Sensitivity DNA Kit (Agilent Technologies, Inc.). The length of barcoded sequencing libraries ranged from 200 to 350 bp. Template preparation for clonal amplification of up to 8 libraries at a concentration of 60 pM and loading of the Ion PI Chip v3 were achieved using the Ion Chef instrument and Ion PI Hi-Q Chef Kit (ThermoFisher Scientific Inc.). Sequencing was performed using the Ion Torrent Proton sequencer (ThermoFisher Scientific Inc.).

## 2.7. Determination of differentially expressed genes

The IonXpress count files were used as the input for DESeq2 [31]. Only genes with at least 10 mapped reads were considered in the subsequent analysis. The standard procedures using the Wald test were applied. The results were created after contrasting selected samples of BCPAP or TPC1 cells, with the adjusted  $p$  value set at 0.05. The following comparisons were performed: i) BCPAP siNEG vs BCPAP siPDPN (named B\_N/B\_P), ii) TPC1 siNEG vs TPC1 siPDPN (named T\_N/T\_P), iii) BCPAP siNEG vs TPC1 siNEG (named B\_N/T\_N), and iv) BCPAP siPDPN vs TPC1 siPDPN (named B\_P/T\_P), summarized in Table 3.

## 2.8. Gene Ontology terms/Kyoto Encyclopedia of Genes and Genomes/Reactome analysis

The Gene Ontology (GO) terms [32], Kyoto Encyclopedia of Genes and Genomes (KEGG), and Reactome pathways [33] analyses were performed with the pathfindR package [34]. The following databases

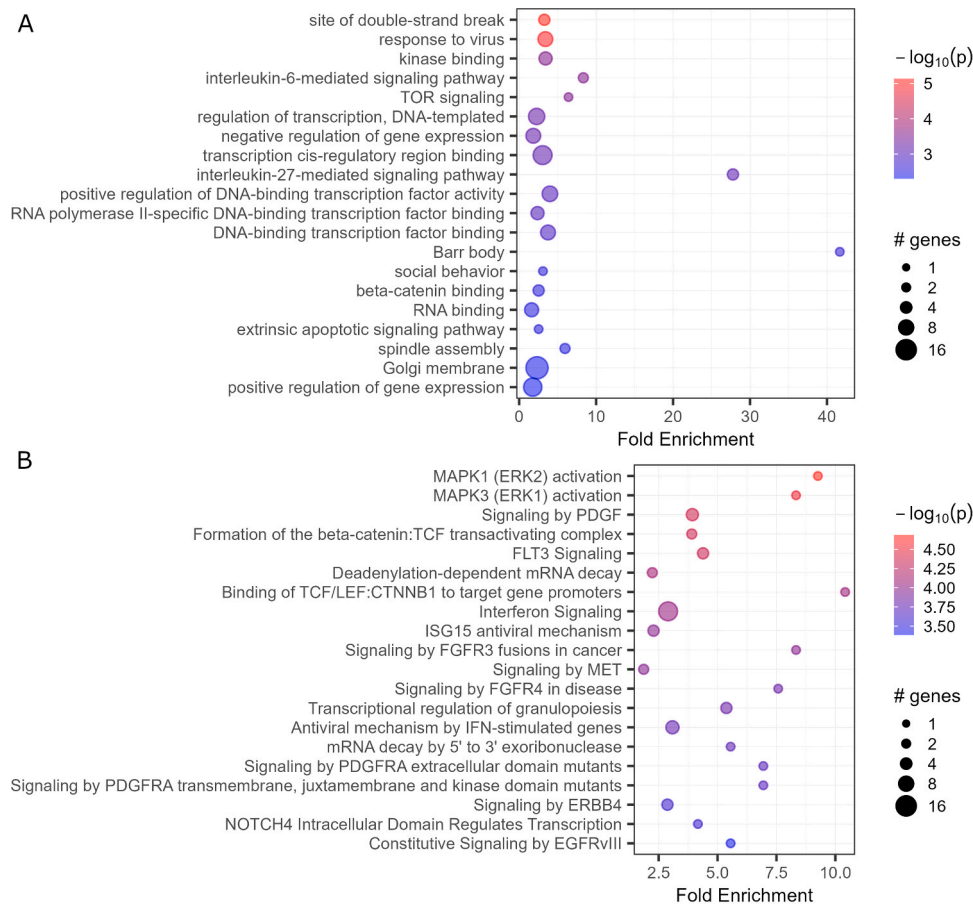


**Fig. 4.** The enrichment analysis of the unique (A) GO terms and (B) Reactome pathways for the B<sub>N</sub>/B<sub>P</sub> comparison. The top 20 most significantly enriched terms and pathways are shown. The size of the bubble corresponds to the number of dysregulated genes; the color refers to the enriched  $p$ -value. Only DEGs with  $|\log_2FC| = > 1.5$  and adjusted  $p$ -value  $< 0.05$  were analyzed.

were used: GO-All, KEGG, and Reactome, with all possible comparisons. Default parameters were applied, with  $p\_val\_threshold = 0.05$ ,  $min\_gset\_size = 5$ ,  $max\_gset\_size = 500$ , and  $enrichment\_threshold = 0.05$ .

## 2.9. Analysis of differentially expressed genes, Gene Ontology terms/ Kyoto Encyclopedia of Genes and Genomes/Reactome pathways

The intersections of differentially expressed genes (DEGs), GO terms, KEGG, and Reactome pathways were generated using custom script in R 4.1.1 project [35]. In all the calculations of the GO terms and KEGG/Reactome pathways, only DEGs with  $|\log_2FC| = > 1.5$  and adjusted  $p$ -value  $< 0.05$  were included in the analyses.

## 2.10. Clustering analysis of differentially expressed genes

The clustering was performed using the R 4.1.1 project [36]. The DEGs characteristic to each of the comparisons were concatenated. Missing values were assigned zero, assuming that the change was not statistically significant. The Euclidean distance matrix was calculated and the hierarchical cluster analysis was performed with `hclust` (method="complete"). The ascribed clusters were visualized separately with the `ggplot2` tool [37].

## 2.11. Heatmaps of genes taking part in migration processes

The DEGs of metabolic pathways directly or indirectly connected to migratory processes were selected. The missing values were assigned zero. Particular groups were clustered and visualized with the `heatmap.2` of `gplots` package and `dist` function for distance matrix computation

(with the Euclidean distance formula).

## 2.12. NF- $\kappa$ B pathway proteome profiling

The assay was performed using the commercial Human NF $\kappa$ B Pathway Array Kit (R&D Systems, Minneapolis, MN, USA), according to the manufacturer's protocol. Briefly, 72 h after transfection, the tested PTC-derived cancer cells transfected with siDPDN or siNEG were washed with ice-cold PBS (pH 7.3) and lysed with designated buffer supplemented with Complete Protease Inhibitor Cocktail (Roche) and Viscolase (A&A Biotechnology). The protein concentration was defined using the BCA Protein Assay Kit (ThermoFisher Scientific Inc.). The array membranes were blocked with Array Buffer 3/6 for 1 h, followed by overnight incubation with 250  $\mu$ g of total protein lysates resuspended in Array Buffer 1 at 4 °C. Next, the membranes were incubated with a Detection Antibody for 1 h at RT and the Streptavidin-HRP solution for 30 min. The chemiluminescent signal was developed using the Chemi Reagent Mix and detected using X-ray films.

## 2.13. Statistical analysis

All experiments were carried out at least three times. The data were analyzed with GraphPad Prism 6.0 (GraphPad, Inc., San Diego, CA, USA). Nonparametric Mann–Whitney U test and one-way ANOVA, followed by Bonferroni *post hoc* comparative test or *t*-student test were used to evaluate statistical significance (considered at  $p$  value  $< 0.05$ ). The quantitative results were presented as mean  $\pm$  standard deviation (SD). In the case of RNA-seq data analysis, data preparations, modifications and graphs were produced using custom R scripts with the R 4.1.1

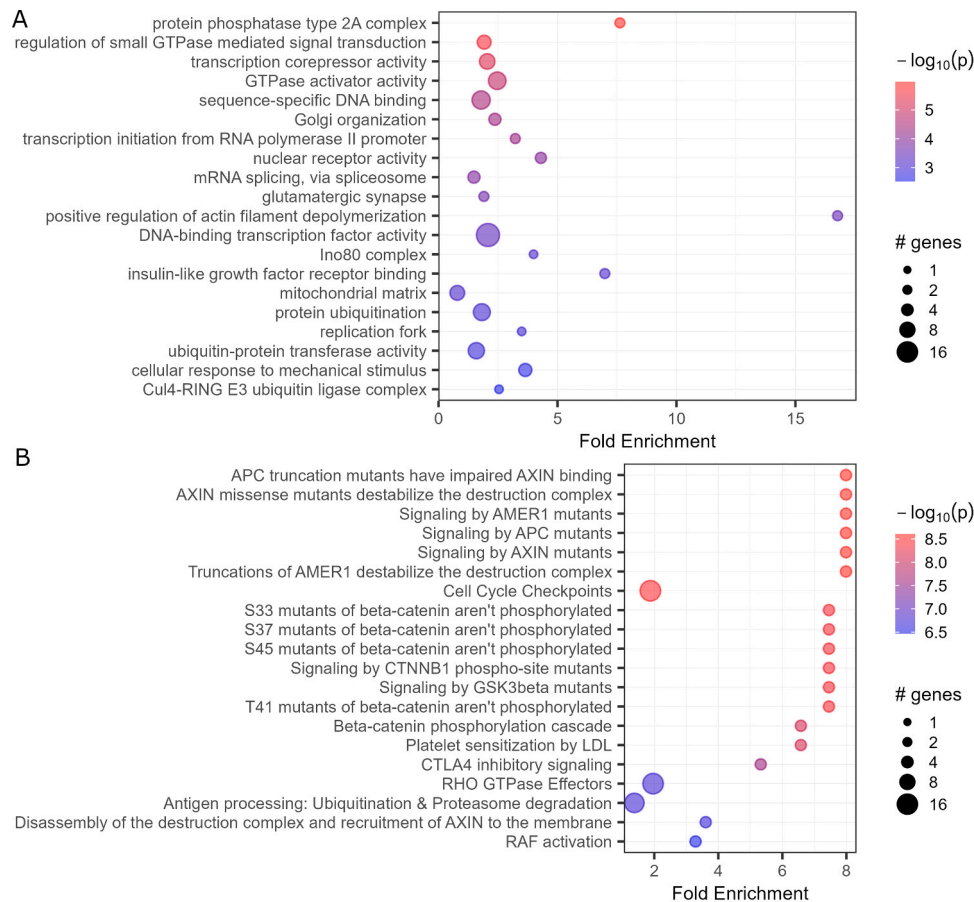


**Fig. 5.** The enrichment analysis of the unique (A) GO terms and (B) Reactome pathways for the T<sub>N</sub>/T<sub>P</sub> comparison. The top 20 significantly enriched terms and pathways are presented. The size of the bubble corresponds to the number of dysregulated genes; the color refers to the enriched  $p$ -value. Only DEGs with  $|\log_2FC| \geq 1.5$  and adjusted  $p$ -value  $< 0.05$  were analyzed.

project [36] and ggplot2 [37].

### 3. Results

#### 3.1. Silencing of PDPN in BCPAP and TPC1 cells

Two model PTC cell lines, TPC1 and BCPAP, were used in the study. BCPAP cells harbor the *BRAF* V600E mutation, while TPC1 cells carry the *RET*/*PTC1* rearrangement. In both cell lines, enhanced *PDPN* expression has previously been shown [11,13]. It was concluded that *PDPN* may act as an important component of the regulatory molecular machinery controlling the metastatic potential of PTC cells, as we observed that the migratory pattern of BCPAP and TPC1 cells can be reversed by knockdown of *PDPN* expression. To further explore this phenomenon, a RNA-seq analysis was implemented. Additionally, the analysis was expanded by linking the observed *PDPN* phenotype with the mutational background of the studied cells.

For RNA-seq analysis, *PDPN* was silenced in both PTC-derived cell lines. The efficiency of *PDPN* depletion was verified by RT-qPCR and Western blot (Fig. 1A and B, respectively). As shown, 8-fold and 10-fold reductions in the expression of *PDPN* were observed in siPDPN-treated TPC1 and BCPAP cells, respectively. It was also confirmed that *PDPN* expression in BCPAP cells is significantly higher than in TPC1 cells.

To assess the distribution of the samples of the TPC1 and BCPAP cells transfected with siPDPN or siNEG, a principal component analysis (PCA) was performed. A clear separation of all variants was observed (Fig. 2).

#### 3.2. The impact of podoplanin expression on the transcriptome of the studied PTC-derived cells

The subsequent DEGs analysis enabled determination of the transcriptome profiles of BCPAP and TPC1 cells with wild-type or depleted expression of *PDPN*. For this purpose, the gene expression data obtained for each tested set were contrasted: TPC1 siNEG vs TPC1 siPDPN (T<sub>N</sub>/T<sub>P</sub>) and BCPAP siNEG vs BCPAP siPDPN (B<sub>N</sub>/B<sub>P</sub>), and the DEGs were revealed. All the acquired DEGs are listed in File S1.

Among the 584 DEGs revealed for BCPAP, 227 of them were up- and 357 down-regulated. In the case of the TPC1 set, among all the revealed DEGs (832), 443 of them were up- and 389 down-regulated, respectively (Fig. 3A, File S1). The two studied cell lines shared 259 DEGs, and among them 83 were up- and 175 down-regulated.

RNA-seq data was validated using real time RT-qPCR. Ten significantly dysregulated (up- or down-regulated) genes were randomly selected and expression values calculated for real time RT-qPCR and RNA-seq analyses were compared. Similarities in expression data sets were confirmed for each of the tested genes (File S2).

To further clarify the differences in the migration patterns of the BCPAP and TPC1 cells and the potential role of *PDPN* in this process, functional pathways in the studied cells were determined (Fig. 3B; File S3). The analysis of the association between the dysregulated gene sets and biological processes in the B<sub>N</sub>/B<sub>P</sub> and T<sub>N</sub>/T<sub>P</sub> sets led to identification of 69 and 61 unique terms, respectively, while only 13 GOs were found to be mutual. Reactome pathways analysis indicated a more equal distribution of the identified pathways in the BCPAP set (116 unique vs 91 mutual), while a larger difference in the TPC1 set (194 unique vs 91 shared) was observed. In contrast, most of the KEGG pathways were

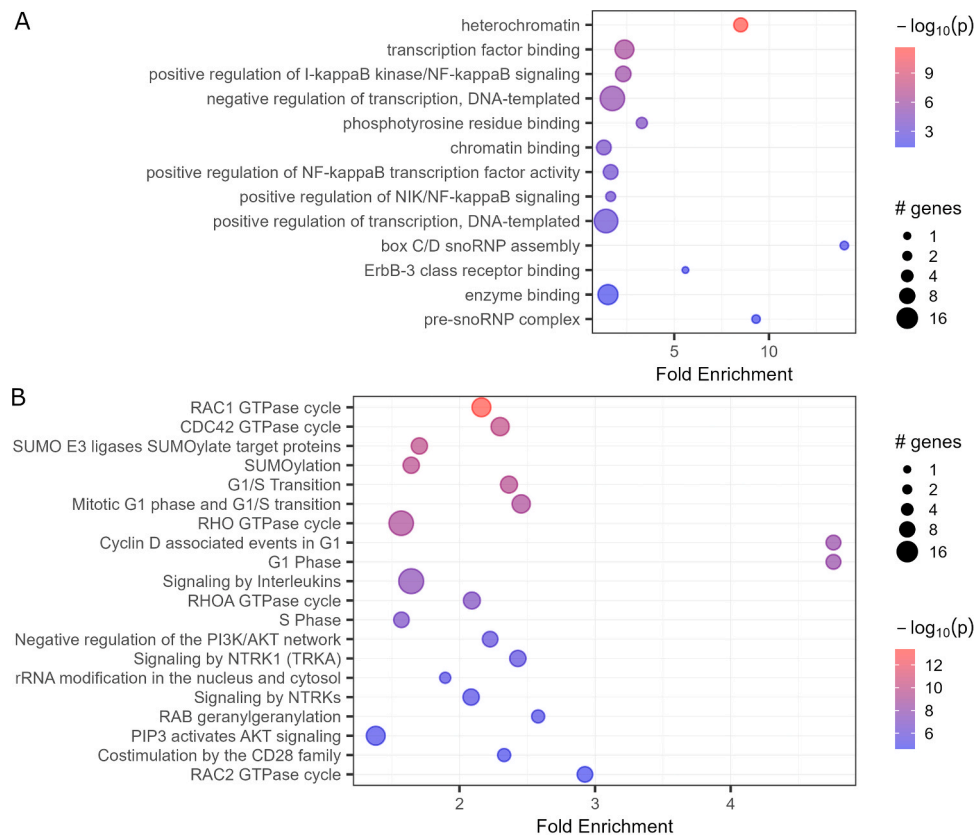


**Fig. 6.** The enrichment analysis of the shared (A) GO terms and (B) Reactome pathways for the B<sub>N</sub>/B<sub>P</sub> and T<sub>N</sub>/T<sub>P</sub> comparisons. Up to 20 significantly enriched terms and pathways are shown. The size of the bubble corresponds to the number of dysregulated genes; the color refers to the enriched  $p$ -value. Only DEGs with  $|\log_2FC| = > 1.5$  and adjusted  $p$ -value  $< 0.05$  were analyzed.

found to be mutual (88 out of 122 and 117 for BCPAP and TPC1, respectively).

Further analysis of non-mutual GO terms, KEGG, and Reactome pathways revealed substantial differences in the tested sets, including pathways related to migration and invasion (File S4). The most significantly enriched terms and pathways are summarized in Figs. 4–6. In the analyzed BCPAP cells (B<sub>N</sub>/B<sub>P</sub> comparison), terms associated with transcriptional and translational regulation processes and migration, *i. e.*: TOR signaling or  $\beta$ -catenin binding, were identified (Fig. 4A). This observation was supported by data from the Reactome analysis, which divulged more pathways related to cell migration, such as the MAPK1 and MAPK3,  $\beta$ -catenin-mediated Wnt signaling (transactivating complex  $\beta$ -catenin/T-cell factor), interferon (IFN) signaling, FGFR signaling (by FGFR3 fusion and FGFR4), or EGFR signaling (by ERBB4 and EGFRvIII) pathways (Fig. 4B).

The GO terms mined for the T<sub>N</sub>/T<sub>P</sub> comparison mainly represented genes involved in transcriptional and translational regulation processes. Moreover, multiple terms were associated with metastasis, such as regulation of actin filament depolymerization (significantly enriched), lamellipodium assembly, small GTPase-mediated signal transduction and GTPase activating proteins, and the  $\beta$ -catenin phosphorylation cascade (Fig. 5). Similarly, the Reactome pathway enrichment analysis revealed multiple pathways involved in cell migration, including WNT/ $\beta$ -catenin, GSK3, MAPK, and RHO GTPase signaling pathways (Fig. 5B).

Additionally, the B<sub>N</sub>/B<sub>P</sub> and T<sub>N</sub>/T<sub>P</sub> sets were compared. The GO terms common for both sets were associated with NF- $\kappa$ B signaling pathway (Fig. 6A), while the most significantly enriched Reactome pathway was the PI3K/AKT signaling pathway, including its molecular stimulators (RAS, CDC42 or RHO GTPases) (Fig. 6B).

### 3.3. Analysis of the role of the molecular background on the transcriptome of the studied PTC-derived cells

The following step aimed to evaluate the potential relationship between the molecular background (presence of *BRAF* V600E or *RET*/*TPC1* alterations) of the studied PTC cells and the status of *PDPN* expression. We assumed that such an analysis may provide information regarding differences in the intracellular signaling network that lead to the divergent migratory properties of BCPAP and TPC1 cells. For this purpose, the DEGs were identified for the BCPAP siNEG vs TPC1 siNEG (B<sub>N</sub>/T<sub>N</sub>) and BCPAP siPDPN vs TPC1 siPDPN (B<sub>P</sub>/T<sub>P</sub>) sets. All the acquired DEGs are listed in File S2.

The comparisons of the BCPAP and TPC1 wild-type cells expressing *PDPN* (B<sub>N</sub>/T<sub>N</sub>) led to the identification of 1726 up- and 1166 down-regulated DEGs. Similarly, the examination of the B<sub>P</sub>/T<sub>P</sub> set revealed 1705 up- and 989 down-regulated DEGs (Fig. 7A).

Interestingly, for cells with wild-type and silenced *PDPN*, most DEGs (2171) were shared and among those overlapped genes, 1361 were up-regulated, while 810 were down-regulated (Fig. 7A). It was found that 721 DEGs were unique for wild-type cells expressing *PDPN* (B<sub>N</sub>/T<sub>N</sub> set), and among them 365 were up- and 356 down-regulated. A similar number of unique DEGs (523 in total; 344 up- and 179 down-regulated) was found for the *PDPN*-silenced BCPAP and TPC1 cells (B<sub>P</sub>/T<sub>P</sub> set) (Fig. 7A).

Moreover, the comparison analysis of the B<sub>N</sub>/T<sub>N</sub> and B<sub>P</sub>/T<sub>P</sub> sets (addressing the molecular background) revealed that the most terms (161) and pathways (115 KEGG and 196 Reactome) were mutual (Fig. 7B; File S5). Among the overlapping GO terms (B<sub>N</sub>/T<sub>N</sub> and B<sub>P</sub>/T<sub>P</sub> sets), mainly those responsible for positive or negative regulation of transcription, regulation of cell cycle, or protein phosphorylation were identified (Fig. 8; File S4). The Reactome pathway analysis of mutual

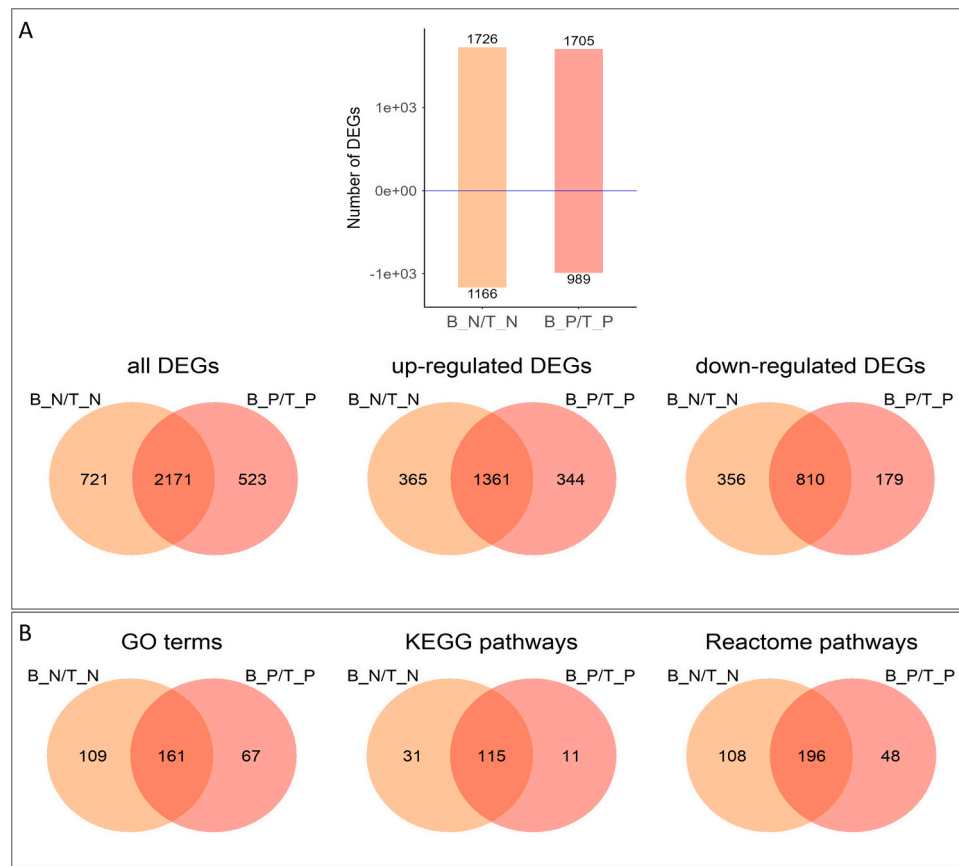


**Fig. 7.** A) The number of DEGs for the: B\_N/T\_N (BCPAP siNEG vs TPC1 siNEG) and B\_P/T\_P (BCPAP siPDPN vs TPC1 siPDPN) comparisons. B) The number of unique and common GO terms, KEGG, or Reactome pathways for the comparisons showing the impact of the genetic background (B\_N/T\_N and B\_P/T\_P). Only DEGs with  $|\log_2FC| > 1.5$  and adjusted  $p$ -value  $< 0.05$  were analyzed.

DEGs showed enrichment in *e.g.* post-translational modification (SUMOylation of intracellular receptors), nuclear receptor transcription pathway, or PI3K/AKT signaling. Additionally, GO terms or Reactome pathways connected with cell migration, such as actin binding, cell junction, extracellular matrix organization, integrin cell surface interaction, MAPK signaling, as well as RHO, CDC42, and RAC1 GTPase cycles, were mined (Fig. 8).

The subsequent analysis of unique GO terms and Reactome pathways in the B\_N/T\_N set showed that bicellular tight junctions, protein localization to cell-cell junction, or structural constituents of cytoskeleton were most significantly enriched (Fig. 9A). Moreover, the mined EPHA-mediated growth cone collapse indicated the involvement of the ephrin receptor that can potentially lead to the activation of citron kinase (CIT), a paralog of the RHO kinase (ROCK), or inactivation of RAC1 (Fig. 9B). Overall, the observed uniquely dysregulated pathways are mainly related to processes linked with the regulation of cell motility.

Also, the mined data from the unique GOs and Reactome pathways in the B\_P/T\_P set (after PDPN silencing) were abundant in terms and pathways related to signaling involved in migration, such as actin filament bundle assembly, ERK1 and ERK2 cascade, transmembrane receptor protein kinase signaling, or the Toll-like Receptor 2 (TLR2) cascade involving My88:MAL, which can lead to the activation of RAC1, AKT, or RUNX3 in regulation of WNT signaling (Fig. 10).

### 3.4. Clustering of DEGs

The obtained data generally describe the changes in gene expression in BCPAP and TPC1 cells due to modulations in PDPN yield (B\_N/B\_P vs T\_N/T\_P). Moreover, the role of the molecular background in PDPN-expressing and PDPN-non-expressing PTCs in regulation of cell

migration was also addressed (B\_N/T\_N vs B\_P/T\_P). It was found that in each analyzed set some of the overlapping genes appeared to present opposite expressional patterns, which suggested that they can be regulated via various mechanisms or may be involved in different response pathways (regarding the presence or absence of PDPN).

To further investigate this phenomenon, we performed clustering of DEGs identified in the B\_N/B\_P vs T\_N/T\_P and B\_N/T\_N vs B\_P/T\_P sets (File S6 and S7). The analysis was completed separately for both sub-groups (for values  $|\log_2FC| > 1.5$  and adjusted  $p$ -value  $< 0.05$ ). We especially focused on transcription factors and genes associated with cell metastasis. Selected overlapping DEGs in the B\_N/B\_P and T\_N/T\_P groups were clustered based on changes in the gene expression value (Fig. 11). The analysis revealed 14 genes that presented characteristic expressional trends, as they were up-regulated in the B\_N/B\_P and down-regulated in the T\_N/T\_P group (Fig. 11, cluster 3; File S8 and S9). Among them, genes linked with cell adhesion and migration were identified, including *ADD3* ( $\gamma$ -adducin; affecting cell-cell junctions), *CLDN1* (claudin-1; inducing tight junctions), *DEPDC7* (encoding a putative signal transduction protein involved in NF- $\kappa$ B activation, the dysregulation of which leads to cancer migration), or *NUAK1* (a serine/threonine-protein kinase involved in the promotion of tumor metastasis under regulation by AKT1).

On the other hand, 28 genes were found to be up-regulated in the T\_N/T\_P set (when compared to the B\_N/B\_P group; Fig. 11, cluster 5). Those up-regulated genes comprised *e.g.* *ANTXR2* (involved in interactions with laminin and the extracellular matrix), *ARL14EPL* (a homolog of ARL14EP, which interacts with ARL14,  $\beta$ -actin, and myosin 1E), *NGEF* (engaged in the ephrin receptor signaling and control of cytoskeletal organization via activation of RHOA and RHOB proteins), significantly dysregulated *NOX5* (a NADPH oxidase activating the c-Abl

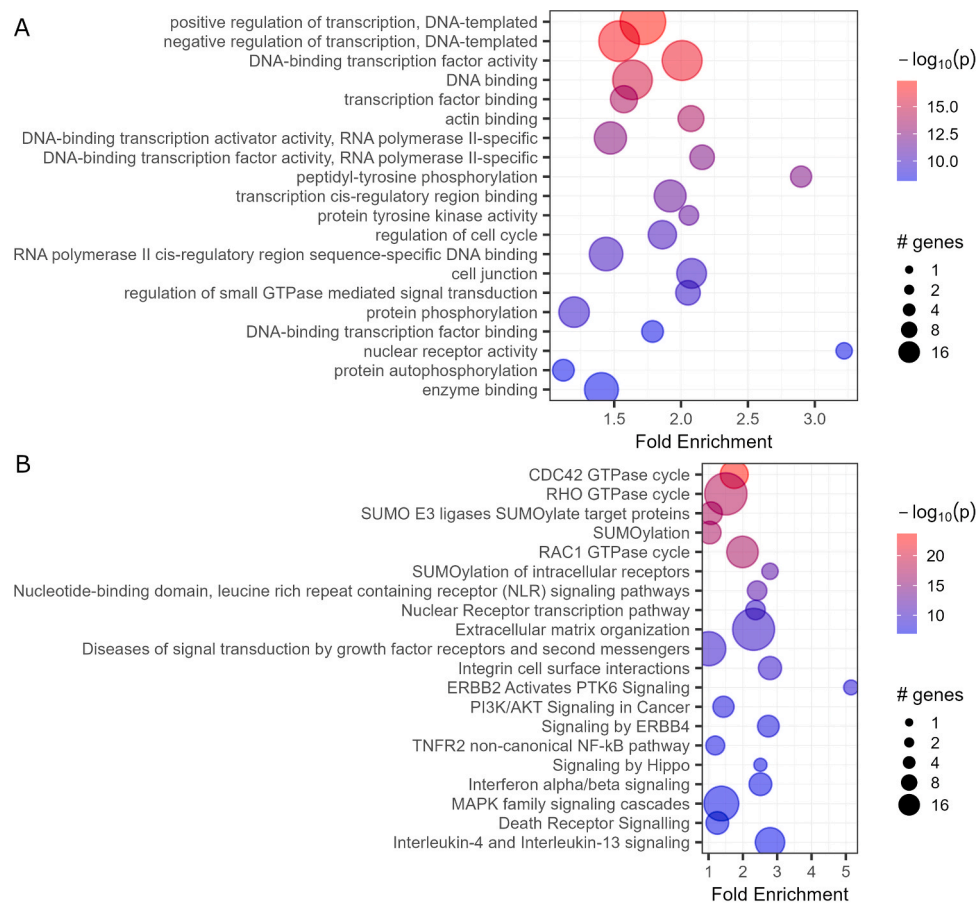


**Fig. 8.** The enrichment analysis of (A) GO terms and (B) Reactome pathways among the shared B<sub>N</sub>/T<sub>N</sub> and B<sub>P</sub>/T<sub>P</sub> comparisons. The 20 most significantly enriched terms and pathways are shown. The size of the bubble corresponds to the number of dysregulated genes; the color refers to the enriched  $p$ -value. Only DEGs with  $|\log_2FC| > 1.5$  and adjusted  $p$ -value  $< 0.05$  were analyzed.

kinase by reactive oxygen species production, which leads to the modification of several signaling pathways) and *SEMA7A* (inducing cellular EMT), or *SHANK1* (interacting with ARHGGEF7 and thus activating RAC1 and CDC42 GTPases, master regulators of various processes including migration, adhesion, and cytoskeleton organization).

Next, the clusters of DEGs common for the B<sub>N</sub>/T<sub>N</sub> and B<sub>P</sub>/T<sub>P</sub> groups (reflecting the impact of the molecular background; Fig. 12) were evaluated. We especially focused on clusters 3 and 4. The analysis of expression patterns of DEGs revealed groups of genes down-regulated in the B<sub>N</sub>/T<sub>N</sub> but up-regulated in the B<sub>P</sub>/T<sub>P</sub> subsets (Fig. 12A, cluster 3 and Fig. 12B), suggesting that the expression of this set of genes is linked to the PDPN status. Among the 21 identified genes, a significant fraction was involved in signal transduction, including *FZD8* (a receptor for WNT and a member of the  $\beta$ -catenin signaling pathway), *IGFBP6* (activator of the MAPK signaling cascade and cell migration), *KLF2* (activated by MEK5/ERK5, downregulating the endothelial cell adhesion molecules VCAM1 and SELE), *RIN1* (interacting with HRAS, thus remodeling the cytoskeleton), *RRM2* (an inhibitor of WNT signaling), and *SPSB1* (directly interacts with MET tyrosine kinase and affects c-MET signaling).

Interestingly, 6 genes showing an inverted expressional pattern (up-regulated in the B<sub>N</sub>/T<sub>N</sub> and down-regulated in the B<sub>P</sub>/T<sub>P</sub> set) were revealed. Among them, *ADAMTSL3*, as well as *DEPDC7* and *SAA1* (also found in cluster 3), are involved in extracellular matrix organization. The other identified genes were *DANCR* (differentiation antagonizing non-protein coding RNA), *TSPAN18* (tetraspanin 18), and *APH1B* (implicated in the  $\gamma$ -secretase complex).

Considering all the described clusters, many genes encoding for proteins directly or indirectly connected to cell junction formation or

migration were recognized.

### 3.5. Podoplanin and PTC-driving mutations affect the expression of genes involved in cell migration

Here, we further investigated the selected overlapping genes in the analyzed sets (B<sub>N</sub>/B<sub>P</sub> vs T<sub>N</sub>/T<sub>P</sub> and B<sub>N</sub>/T<sub>N</sub> vs B<sub>P</sub>/T<sub>P</sub>), which were found to be linked with cell migration processes. Heatmaps of the expression values of the analyzed genes were generated.

Analysis of the RAS/MAPK pathway (Fig. 13A) indicated major changes in the expression of the *RASD2* and *RASSF9* genes in the BCPAP cells. The wild-type expression of *PDPN* in BCPAP cells (B<sub>N</sub>/B<sub>P</sub> comparison) showed reduced levels of *RASD2* and *RASSF9* ( $-2.4$  x), while no effect was observed in the TPC1 cells. Also, *RRAS2* was up-regulated ( $0.6$  x), while *KRAS* was down-regulated ( $-1.8$  x) in the B<sub>N</sub>/B<sub>P</sub> comparison without any significant change in the TPC1 cell lines. The expression of the *RASSF8*, *RASSF7*, *RASA3*, *TRAF* and *ARAF* genes changed depending on the cell line. In TPC1 cells (T<sub>N</sub>/T<sub>P</sub> comparison) it was elevated ( $1.0$  x,  $1.4$  x,  $0.6$  x,  $0.8$  x, and  $0.7$  x, respectively), while in BCPAP cells it remained unchanged. On the other hand, *RASAL2* and *TRAF3IP2* were down-regulated in wild-type TPC1 cells.

As expected, the expression of the members of the PI3K/AKT pathway was also altered (Fig. 13B). Most importantly, *PTENP1* was overexpressed ( $3.9$  –  $4.4$  x), while *PIK3CG* and *PIK3IP1* were inhibited ( $-1.7$  to  $3.9$  x) in cells with *BRAF* V600E. In BCPAP cells with wild-type expression of *PDPN*, the *PIK3CG* gene was triggered ( $0.9$  x). The expression of *RICTOR*, *MTOR*, or *AKT3* was slightly induced in the presence of the *BRAF* V600E, which stays in contrast to the cells with wild-type *PDPN* expression. Moreover, in TPC1 wild-type cells, *PIK3IP1*,

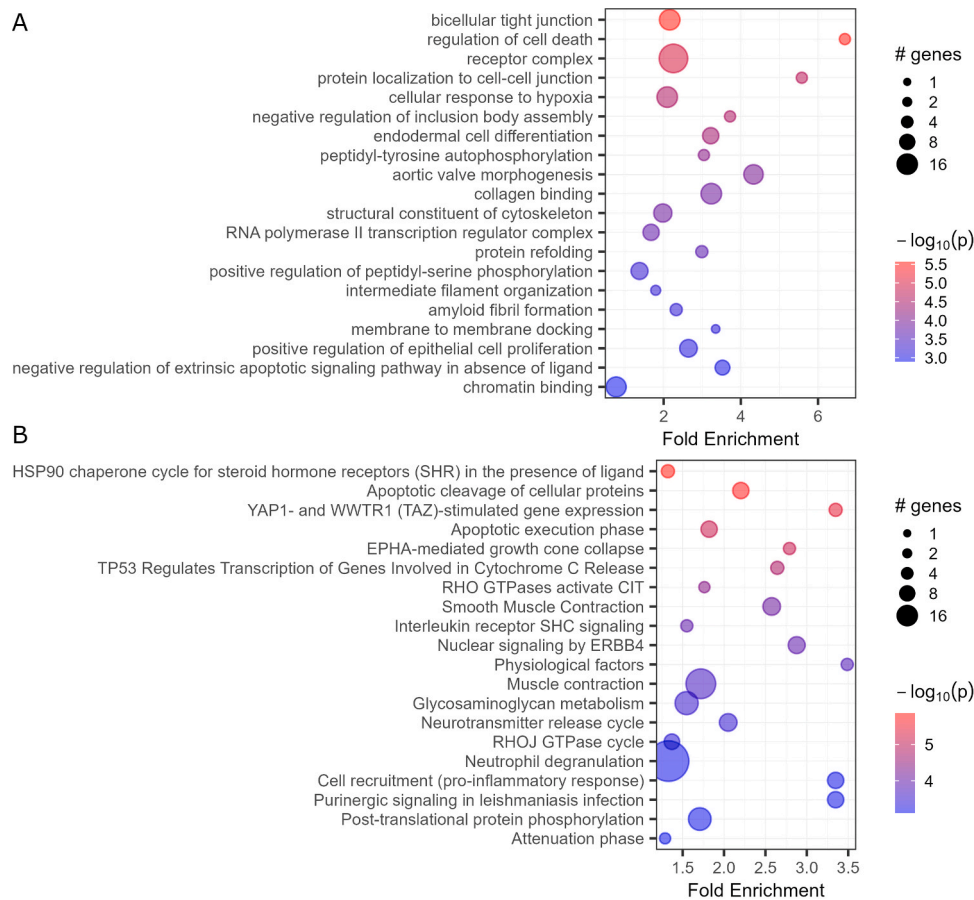


**Fig. 9.** The enrichment analysis of unique (A) GO terms and (B) Reactome pathways for the B\_N/T\_N comparison. The 20 most significantly enriched terms and pathways are presented. The size of the bubble corresponds to the number of dysregulated genes; the color refers to the enriched  $p$ -value. Only DEGs with  $|\log_2FC| \geq 1.5$  and adjusted  $p$ -value  $< 0.05$  were analyzed.

*PIK3R4*, *LAMTOR3*, and *AKTIP* were down-regulated ( $-1.8$  x,  $-1$  x,  $-1.4$  x, and  $-0.5$  x respectively), while *AKT1S1* and *PIK3CD* were up-regulated (1.5 and 0.8 x, respectively). Interestingly, a fraction of dual-specificity phosphatases (DUSP) were suppressed in the B\_N/B\_P comparison (*DUSP4*, *DUSP19*, and *DUSP22*), but up-regulated (*DUSP8* and *DUSP12*) in the T\_N/T\_P set (Fig. 13C).

The main contributors to the process of cell migration are RHO family GTPases, including RAC1 and RHOA. Among them, the expression of the *RHOBTB1*, *RHOJ*, and *RND2* genes was increased in BCPAP cells with wild-type expression of *PDPN*, while expression of *PAK2* was down-regulated. On the other hand, *RHOBTB3*, *ROCK1*, *ROCK2*, *RHOQ*, and *PAK3* were inhibited in wild-type TPC1 cells. However, *RELA*, *RELN*, and *RAC2* were elevated (Fig. 13D and E).

Furthermore, in TPC1 cells the unique, and probably the most clearly visible, changes in gene expression of proteins belonging to the guanine nucleotide exchange factors (GEFs/ARHGGEFs) and GTPase-accelerating proteins (GAPs/ARHGAPs) families were observed (Fig. 13F and G). The majority of those genes were down-regulated (*DOCK10*, *DOCK11*, *ARHGFE6*, *ARHGFE26*, *ARHGFE28*, *ARHGAP12*, and *WASF3*), however *ARHGFE2*, *ARHGFE10L*, *ARHGAP23*, and *ARHGAP27* were up-regulated. Moreover, in BCPAP with wild-type *PDPN* level, expression of *ARHGFE40* and *DOCK2* was elevated, while *WASF1* was inhibited. In contrast to the cells with wild-type expression of *PDPN* (B\_N/T\_N comparison), there is a substantial fraction of RHO GEFs that are up-regulated in *BRAF* V600E cells (B\_P/T\_P set), especially *ELMOD1*, *TIAM2*, and *DOCK2* (3.3 – 6.1 x), while others are down-regulated, including *TIAM1* and *ARHGFE12* ( $-1.3$  to 2.7 x). Importantly, *PREX1* (phosphatidylinositol 3,4,5-trisphosphate-dependent RAC exchanger 1 protein) is substantially up-regulated in *PDPN* expressing cells (6.5 – 6.8 x; B\_N/B\_P

and T\_N/T\_P sets; Fig. 13F). On the other hand, the group of RHO GTPase activating ARHGAPs (Fig. 9G) can be divided into two subsets, one presenting substantially up-regulated GAPs, e.g., *ARHGAP24* and *ARHGAP25* (6.1 – 10.1 x), and the other generally down-regulated, e.g., *ARHGAP6* ( $-4.9$  to 6.7 x). This stays in contrast to the wild-type cells, where changes in expression of GAPs seem to be non-significant.

We also evaluated the effect of *PDPN* silencing on the molecular background of both PTC-derived cell lines. Notable upregulation of *RASD2* (3.8 x) and *RASSF8* (1.7 x) or downregulation of *TRAF3IP2* ( $-1.5$  x) gene expression was observed in the B\_P/T\_P comparison (Fig. 13A). Moreover, the expression of the *PIK3R2*, *PIK3R3*, and *PIK3CB* genes of the AKT pathway was down-regulated in the mentioned comparison. Interestingly, one of the components of the DUSP pathway, *DUSP9*, was significantly dysregulated in the B\_N/T\_N set, with no difference in the B\_P/T\_P comparison (Fig. 13C). Also, significant changes in the expression of genes belonging to the RHO pathway were also found. Among them, *RHOBTB2* expression was augmented, while expression of *RHOT2*, *RHOBTB1*, *RHOV*, and *ROCK2* was impaired in the B\_P/T\_P set (Fig. 13D). In addition, the *DOCK2* gene of the ARHGEF pathway and *ARHGAP36* of the ARHGAP pathway were up-regulated, whereas *ARHGAP19* was down-regulated (Fig. 13F and G).

It was considered that the mentioned genes may be downstream effectors of *PDPN* activity and some of them may be responsible for the different response patterns of wild-type and *PDPN*-silenced BCPAP and TPC1 cells.

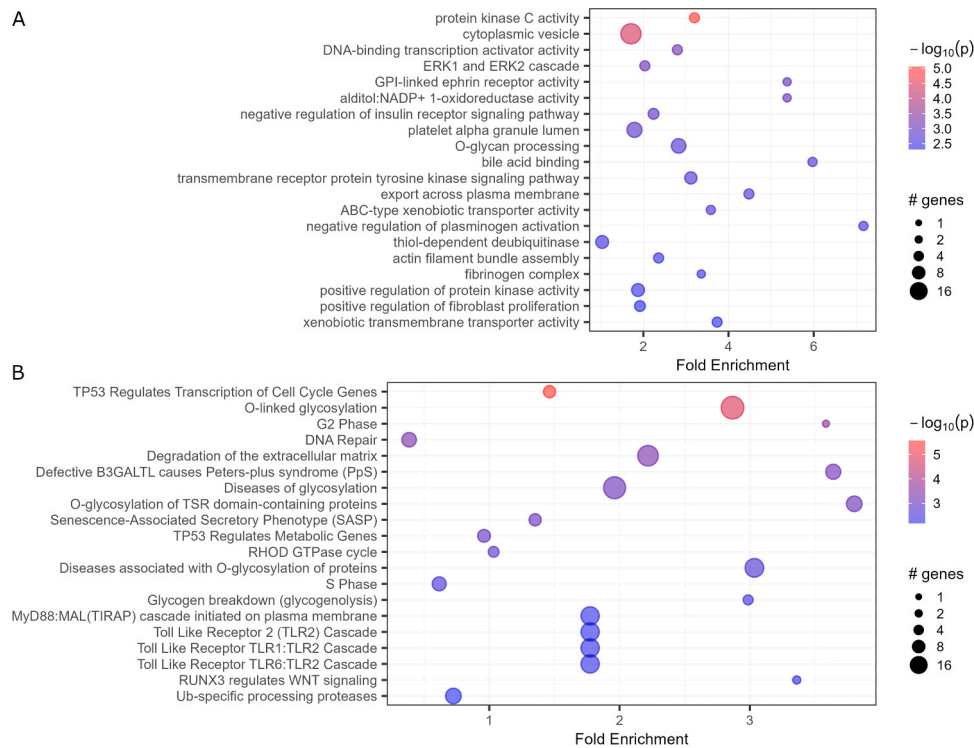


**Fig. 10.** The enrichment analysis of unique (A) GO terms and (B) Reactome pathways for the B\_P/T\_P comparison. The 20 most significantly enriched terms and pathways are shown. The size of the bubble corresponds to the number of dysregulated genes; the color refers to the enriched  $p$ -value. Only DEGs with  $|\log_2FC| > 1.5$  and adjusted  $p$ -value  $< 0.05$  were analyzed.

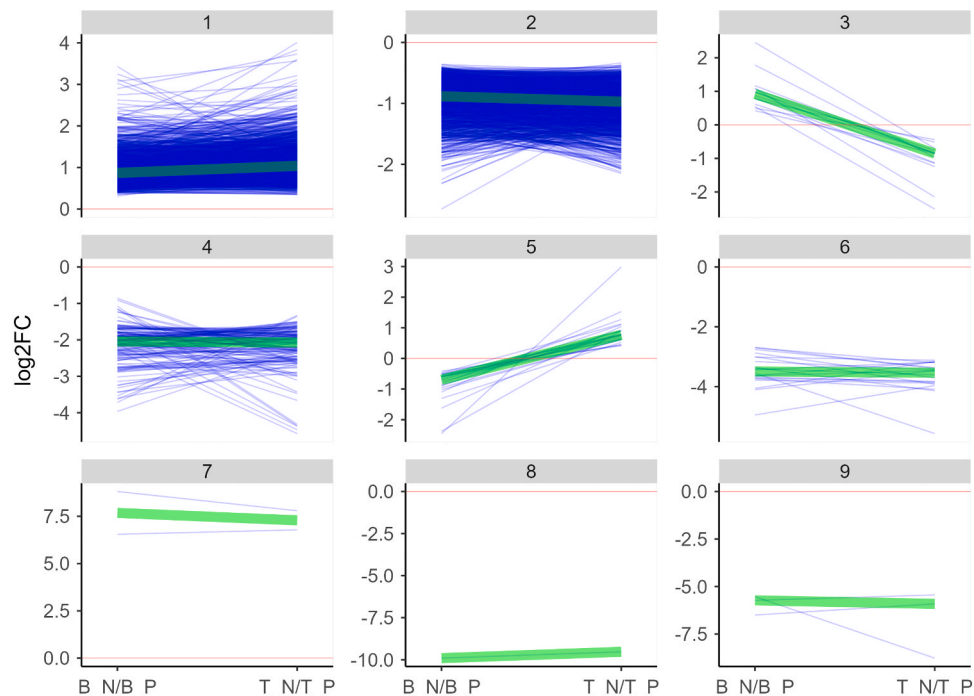


**Fig. 11.** The clusters of DEGs show different expression patterns in the B\_N/B\_P and T\_N/T\_P groups. Each cluster represents the expression of a selected group of genes. The blue line reflects a single gene. The green line represents the mean of all presented genes for each cluster. Clusters 3 and 5 show the contrasting patterns in gene expression. Only DEGs with  $|\log_2FC| > 1.5$  and adjusted  $p$ -value  $< 0.05$  were analyzed.

**3.6. The status of the NF- $\kappa$ B pathway is affected by PDPN expression or the presence of the BRAF V600E mutation**

commercial proteome profiler allowed for detection of 24 proteins with altered levels in BCPAP and TPC1 cells deficient in PDPN. It was found that all the affected proteins belonged to the NF- $\kappa$ B pathway.

A detailed analysis of selected signaling pathways using a

Overall, the BRAF-mutated BCPAP cells presented an increased level

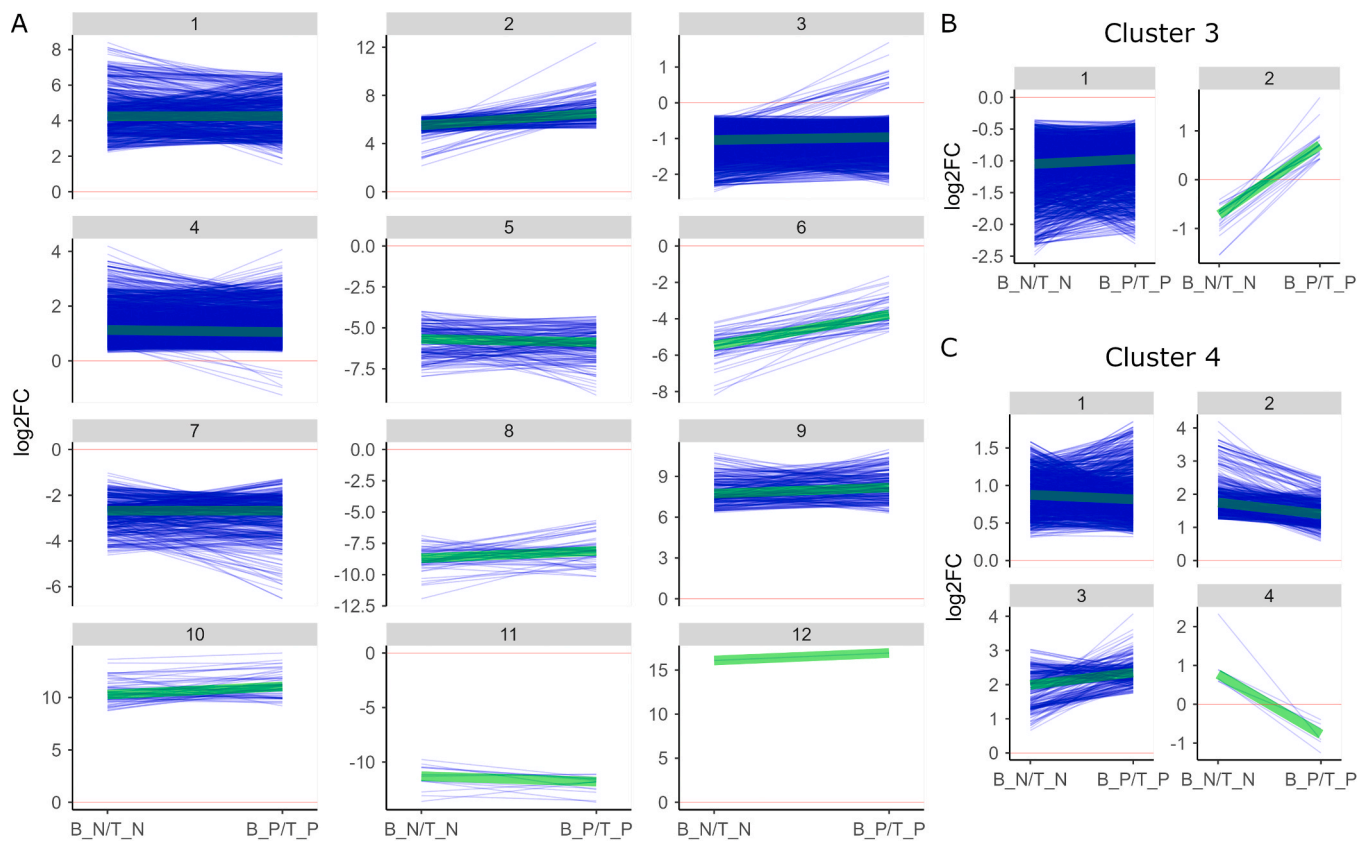


**Fig. 12.** The clusters of DEGs present a different expression pattern among the B\_N/T\_N and B\_P/T\_P groups. Detailed analysis of clusters 3 and 4 (from panel A3 and A4, respectively) is shown on panels B and C. Each cluster represents the expression of a selected group of genes. The blue line reflects a single gene. The green line represents the mean of all presented genes for each cluster. Only DEGs with  $|\log_2FC| > 1.5$  and adjusted  $p$ -value  $< 0.05$  were analyzed.

of apoptosis-associated speck-like proteins, including: ASC, P53 (pS46), STAT2 (pY689), and TNFRSF1B, regardless of the *PDPN* expressional level. On the other hand, proteins presenting reduced level, such as dAP2 and IL-17 RA, were also identified.

It was found that despite their endogenous low level, ASC, BCL10, IL-1 RI, MYD88, and c-Rel proteins were enhanced (up to 4-fold) in both *PDPN*-depleted cell lines. Similarly, an increase in the level of IL-18 R $\alpha$  and IRAK1 was observed. However, the level of SHARPIN and TRAIL proteins was decreased.

There was a group of 4 proteins, which presented opposite protein content in the *PDPN*-deficient cells. The expression of RELA, STAT1p91, JNK1/2 (MAPK8/9), and P53 (including P53 (pS46)) was up-regulated in TPC1 siPDPN cells and down-regulated in BCPAP *PDPN*-depleted cells. In contrast, an opposite pattern was observed for NF- $\kappa$ B1.

Among proteins with altered expression in TPC1 siPDPN cells, the level of dAP2 was reduced (by 30%), while IKK2IL-17 was found to be increased. Interestingly, IKK1, SOCS-6, LTBR, and TNF RII were uniquely repressed in BCPAP siPDPN cells. STAT2 (pY689) was the only protein showing increased level in the BCPAP siPDPN cells. All the results are summarized in Fig. 14.

### 3.7. The activity of the MAPK and PI3K/AKT signaling pathways is altered after *PDPN* silencing

To further elucidate the metabolic status of BCPAP and TPC1 cells, including after silencing of *PDPN*, we performed a Western blot analysis of selected kinases (including their active/phosphorylated forms) engaged in signaling pathways of interest. The Western blot analysis showed that in TPC1 cells, the abundance of the phosphorylated form of the AKT kinase (a member of the PI3K pathway) was ~4-fold greater than in BCPAP cells, regardless of siPDPN treatment (Fig. 15). In

contrast, the active form of the ERK kinase (member of the RAS/MAPK pathway) occurred 5-fold more often in BCPAP wild-type cells. Interestingly, *PDPN* silencing resulted in a modest reduction of ERK activity in BCPAP cells, while in TPC1 cells, the observed reduction was substantial.

We also investigated the presence of the active form of the SRC kinase, which is involved in the induction of migratory processes, and we found very high activity levels of SRC in TPC1 cells in comparison to the BCPAP cells. Moreover, in *PDPN*-silenced BCPAP cells, the phosphorylation levels of SRC increased by about 100%.

The analysis of other protein partners of *PDPN*, including CD44 or proteins of the ERM complex, did not reveal any substantial differences in their expression/phosphorylation status. Only a slight increase in the level of CD44 was observed, especially in the BCPAP cells.

## 4. Discussion

In our previous study, we observed a substantial difference in migration patterns between BCPAP and TPC1 cells [11]. Although the two cell lines are derived from the same type of cancer, the oncogenic characteristics are different. BCPAP cells harbor the *BRAF* V600E mutation rendering the MAPK pathway constitutively active. On the other hand, TPC1 cells express a hybrid gene composed of a cytosolic domain of tyrosine kinase RET and CCDC6, leading to the activation of the PI3K/AKT and stimulation of the MAPK pathways [38–40]. Moreover, BCPAP cells exhibit a suppressed migration and invasive potential when compared to TPC1 cells. Surprisingly, when *PDPN* expression was knocked-down, the pattern of migratory properties of cells was found to be reversed and BCPAP cells presented enhanced motility in comparison to TPC1 cells [11]. Therefore, the main goal of the presented study was to elucidate this observation, mainly at the transcriptomic level. We



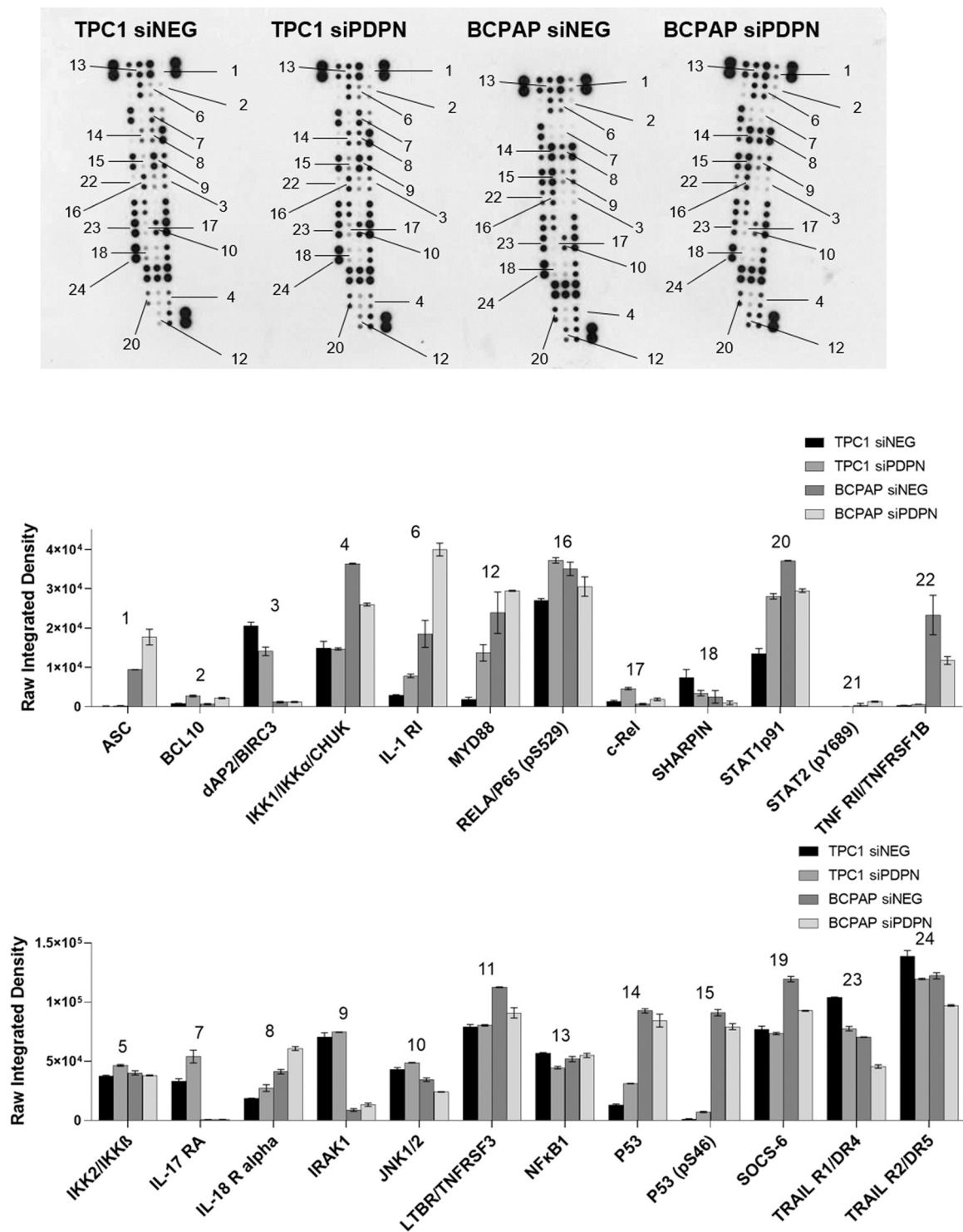


**Fig. 14.** Profile of proteins of the NF-κB pathway was examined after *PDPN* silencing in TPC1 and BCPAP cells. The upper panel shows the developed human NF-κB pathway arrays incubated with protein lysates collected from TPC1 siNEG, TPC1 siPDPN, BCPAP siNEG, and BCPAP siPDPN cells. The results are presented as the mean raw integrated density of two spots ± SD.

ligated to GDP [54]. These two proteins are regulated by the two main signaling pathways, MAPK and PI3K/AKT, and the interplay between them is crucial. We indicated that the reduced motility of wild-type BCPAP cells results from overactivation of RHOA (mediated by enhanced *PDPN* expression) with the simultaneous inability of overactivated MAPK signaling to induce PI3K/AKT and, consequently, RAC1. The statement that RHOA overactivation results in suppressed BCPAP motility is supported by Ward et al. (2019), as it was shown that

in the *PDPN*-positive mesenchymal stromal cells (MSCs), the ROCK inhibitor significantly enhanced the migratory abilities of both control and *PDPN*-silenced cells [55]. Similarly, Lin et al. (2013) observed induction of migration of bone marrow-derived MSCs in the presence of a ROCK inhibitor and an opposite effect in the presence of a PI3K inhibitor [56].

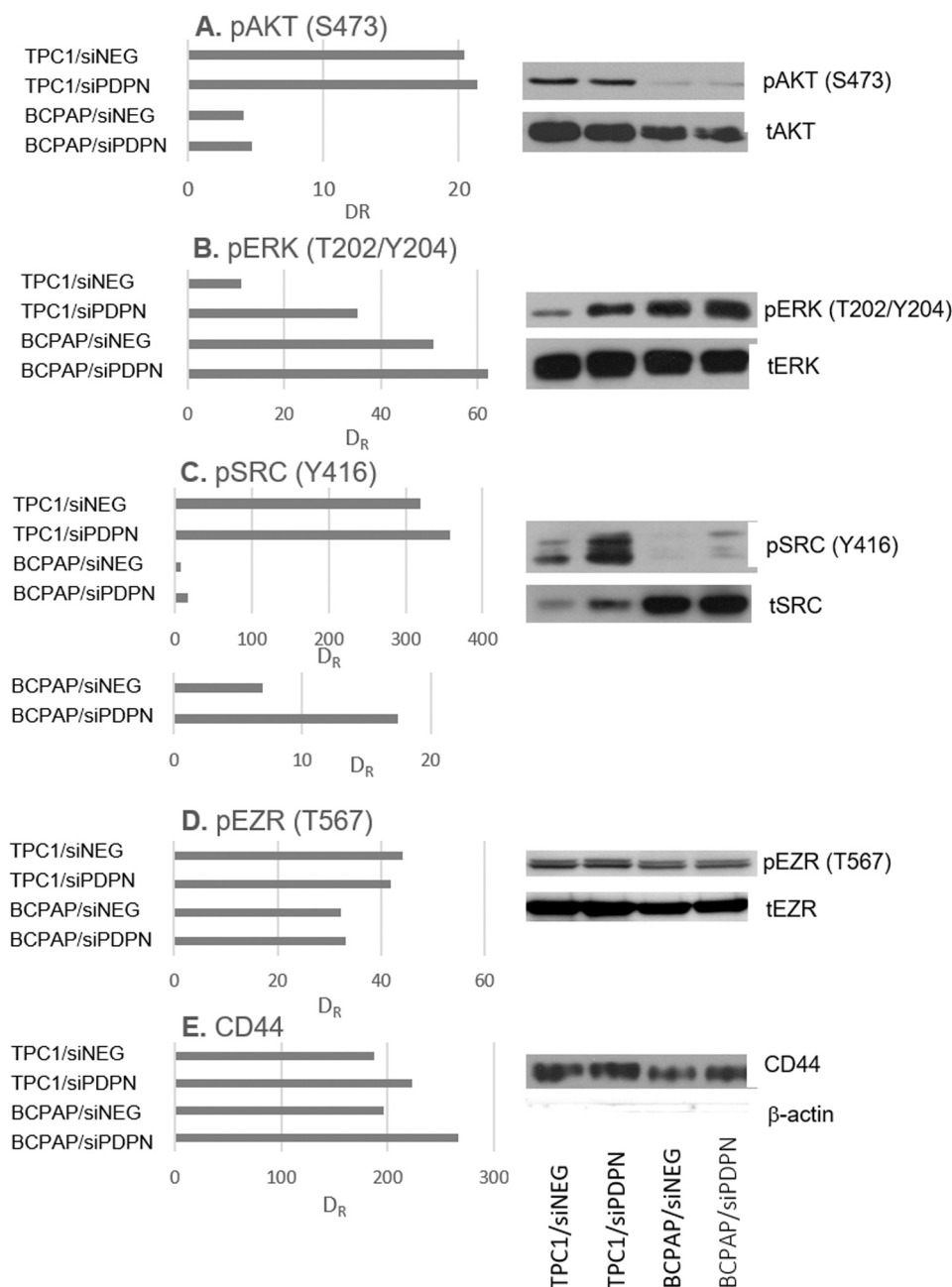


**Fig. 15.** The Western blot analysis and densitometry results of the active (phosphorylated) forms of A) pAKT (S473), B) pERK (T202/Y204), C) pSRC (Y416), D) pEZR (T567), and E) CD44. The densitometry results were normalized to the intensity bands of total corresponding forms (or  $\beta$ -actin for CD44). In the case of the SRC kinase, the subgraph of normalized intensities is shown for BCPAP cells to better visualize small values.  $D_R$ , relative densitometry.

#### 4.3. Role of guanine nucleotide exchange factors and GTPase-activating proteins

Guanine nucleotide exchange factors (GEFs) and GTPase-activating proteins (GAPs) are essential regulators of small G proteins [57]. GEFs activate G proteins through dissociation of GDP, which allows binding of GTP and triggers downstream signaling [57,58]. On the other hand, GAPs turn off signalling events by hydrolysis of GTP [57,59]. The involvement of GEFs and GAPs in the regulation of cell migration pathways is complex. We observed high expression of *TIAM1* (a GEF of RAC1) in TPC1 and low expression of *TIAM2* (a GEF of RHOA) in BCPAP cells expressing *PDPN*. This finding is consistent with the hypothesis of RAC1 activation and can explain the high motility of TPC1 cells.

PREX1 is another GEF of RAC1 that is induced in cells expressing

*PDPN*. It is activated by PI3K at the transcriptomic (through *RUNX1*, *PPAR*, and *USF* transcription factors) as well as proteomic level [60–65]. This kind of regulation further supports the hypothesis that in TPC1 cells, the RAC1 GTPase is activated, in contrast to BCPAP cells, where overactivation of the MAPK pathway leads to its inhibition.

It is known that some catenins can regulate GEFs and GAPs. The requirement of activation of p120 catenin (*CTNND1*; through RHOA) for cell motility has been demonstrated [66]. We also found that *CTNND1* is modestly down-regulated when *BRAF* V600E is present (e.g., in BCPAP cells, the motility of which is reduced).

Another factor leading to suppressed migration of wild-type BCPAP cells is *PTEN*, which further inhibits PI3K activity. Our data confirmed substantial overexpression of *PTENP1*, a competing endogenous RNA that promotes the synthesis of *PTEN* [67], in cells with *BRAF* V600E,

thus leading to the inhibition of both the PI3K pathway and RAC1. Interestingly, one of the transcription factors of *PTENP1* is AP-1, a transcriptional regulator of PDPN activated through the MAPK pathway [68].

#### 4.4. Involvement of other genes in motility of BCPAP and TPC1 cells

The clustering analysis of the BCPAP siNEG vs BCPAP siPDPN and TPC1 siNEG vs TPC1 siPDPN comparisons let us reveal a group of genes differentially regulated in the tested sets, many of which are linked to cell migration. In BCPAP cells, genes inducing cell-cell or tight junctions (e.g., *ADD3*, *CLDN1*, *GPR110*, or *NUAK1*), and therefore inhibiting cell motility, were found. In contrast, the same analysis performed for the TPC1 cells showed upregulation of genes leading to increased cell migration, including *NOX5* (a NADPH oxidase generating ROS and thus activating the pro-migratory c-Abl kinase), *SEMA7A* (inducing an EMT), *NGEF* (a paralog of ARHGEF5, taking part in the ephrin receptor signaling pathway), or *SHANK1* (activating  $\beta$ -PIX, ARHGEF7, and PI3K) [69–71].

A group of factors differentially regulated between the two tested cell lines was also identified in the NF- $\kappa$ B-arrays. The activity of RELA, STAT1, JNK1/2, and P53 proteins was increased in TPC1 siPDPN cells and decreased in BCPAP PDPN-depleted cells.

Additionally, the analysis of the PI3K/AKT and MAPK signaling pathways performed using Western blot showed increased activity of AKT and decreased activity of ERK in TPC1 cells expressing PDPN when compared to BCPAP cells. Although PDPN silencing did not have an impact on the level of phosphorylated AKT, the activity of ERK was much more substantially increased in TPC1 cells. These findings support the transcriptomic results, as well as the stated hypothesis.

Servitja et al. (2003) observed a considerable increase in the activity of RAC1, most likely through the TIAM1 and VAV2 GEFs, in cells transfected with active SRC, one of the main kinases responsible for regulation of cell junctions [72]. We also found that phosphorylation of SRC was increased by about 2-fold in BCPAP cells after silencing PDPN. Therefore, activation of SRC can potentially promote migration of BCPAP cells via RAC1 activation [73].

In conclusion, we have demonstrated a different migratory status in BCPAP and TPC1 depending of the level of PDPN. The observed phenomenon of reduced migration of the wild-type PDPN-expressing BCPAP cells can be explained by: 1) the overactivation of RHOA; 2) the overactivation of PTEN; 3) the inability of the BRAF V600E-regulated MAPK pathway to activate RAC1 by PI3K; 4) a negative feedback loop between RHOA and RAC1; and 5) lack of a positive feedback loop between PI3K, RAC1, and dysregulation of several transcription factors.

The findings from our previous and current studies are particularly relevant in the era of personalized medicine and targeted therapies. The results indicate the importance of knowledge of the molecular background of cancer cells, since the outcome of the treatment may strictly depend on the downstream pathways and genes that are altered. However, since the impact of PDPN on cell migration concerns multiple aspects of cellular signaling, identification of genes and pathways involved in migration still needs to be further explored.

#### Funding

Study was supported by internal grant of the Centre of Postgraduate Medical Education with the number 501-1-026-02-2.

#### Acknowledgements

All persons who have made substantial contributions to the work reported in the manuscript (e.g., technical help, writing and editing assistance, general support), but who do not meet the criteria for authorship, are named in the Acknowledgements and have given us their written permission to be named. If we have not included an

Acknowledgements, then that indicates that we have not received substantial contributions from non-authors.

#### Appendix A. Supporting information

Supplementary data associated with this article can be found in the online version at doi:10.1016/j.csbj.2023.07.035.

#### References

- [1] Pula B, et al. Significance of podoplanin expression in cancer-associated fibroblasts: a comprehensive review. *Int J Oncol* 2013;42(6):1849–57.
- [2] Gamera AM, et al. Abstract 3157: p53 inactivation and STAT2 cooperate to enhance migration and metastasis of colon tumor cells. *Cancer Res* 2018;78(13\_Supplement). 3157-3157.
- [3] Krishnan H, et al. Podoplanin: an emerging cancer biomarker and therapeutic target. *Cancer Sci* 2018;109(5):1292–9.
- [4] Martín-Villar E, et al. Podoplanin binds ERM proteins to activate RhoA and promote epithelial-to-mesenchymal transition. *J Cell Sci* 2006;119(Pt 21):4541–53.
- [5] Suzuki H, Kaneko MK, Kato Y. Roles of podoplanin in malignant progression of tumor. *Cells* 2022;11:3.
- [6] Astarita JL, Acton SE, Turley SJ. Podoplanin: emerging functions in development, the immune system, and cancer. *Front Immunol* 2012;3:283.
- [7] Watanabe N, et al. Podoplanin is indispensable for cell motility and platelet-induced epithelial-to-mesenchymal transition-related gene expression in esophagus squamous carcinoma TE11A cells. *Cancer Cell Int* 2020;20(1):263.
- [8] Li J-C, et al. Podoplanin-positive cancer cells at the edge of esophageal squamous cell carcinomas are involved in invasion. *Mol Med Rep* 2014;10(3):1513–8.
- [9] Schwab M, et al. Podoplanin is required for tumor cell invasion in cutaneous squamous cell carcinoma. *Exp Dermatol* 2021;30(11):1619–30.
- [10] Inoue H, et al. Podoplanin promotes cell migration via the EGF-Src-Cas pathway in oral squamous cell carcinoma cell lines. *J Oral Sci* 2012;54(3):241–50.
- [11] Sikorska J, et al. Podoplanin (PDPN) affects the invasiveness of thyroid carcinoma cells by inducing ezrin, radixin and moesin (E/R/M) phosphorylation in association with matrix metalloproteinases. *BMC Cancer* 2019;19(1). 85–85.
- [12] Chihara N, et al. Induction and transcriptional regulation of the co-inhibitory gene module in T cells. *Nature* 2018;558(7710):454–9.
- [13] Rudzińska M, et al. The role of podoplanin in the biology of differentiated thyroid cancers. *PLoS One* 2014;9(5):e96541.
- [14] Grassi E, et al. Current therapeutic strategies in BRAF-mutant metastatic colorectal cancer. *Front Oncol* 2021;11.
- [15] Ratajczak M, Gawel D, Godlewska M. Novel inhibitor-based therapies for thyroid cancer—an update. *Int J Mol Sci* 2021;22:21.
- [16] Yang M, Huang CZ. Mitogen-activated protein kinase signaling pathway and invasion and metastasis of gastric cancer. *World J Gastroenterol* 2015;21(41):11673–9.
- [17] Mukherjee R, et al. Upregulation of MAPK pathway is associated with survival in castrate-resistant prostate cancer. *Br J Cancer* 2011;104(12):1920–8.
- [18] Loo E, et al. BRAF V600E mutation across multiple tumor types: correlation between DNA-based sequencing and mutation-specific immunohistochemistry. *Appl Immunohistochem Mol Morphol* 2018;26(10):709–13.
- [19] Menicali E, et al. Intracellular signal transduction and modification of the tumor microenvironment induced by RET/PTCs in papillary thyroid carcinoma. *Front Endocrinol (Lausanne)* 2012;3:67.
- [20] Romei C, Elisei R. RET/PTC translocations and clinico-pathological features in human papillary thyroid carcinoma. *Front Endocrinol* 2012;3.
- [21] Xing M. BRAF mutation in thyroid cancer. *Endocr-Relat Cancer Endocr Relat Cancer* 2005;12(2):245–62.
- [22] Prescott JD, Zeiger MA. The RET oncogene in papillary thyroid carcinoma. *Cancer* 2015;121(13):2137–46.
- [23] Henderson YC, et al. High rate of BRAF and RET/PTC dual mutations associated with recurrent papillary thyroid carcinoma. *Clin Cancer Res* 2009;15(2):485–91.
- [24] Liu C, Chen T, Liu Z. Associations between BRAFV600E and prognostic factors and poor outcomes in papillary thyroid carcinoma: a meta-analysis. *World J Surg Oncol* 2016;14(1):241.
- [25] Li J, et al. The BRAF V600E mutation predicts poor survival outcome in patients with papillary thyroid carcinoma: a meta analysis. *Int J Clin Exp Med* 2015;8(12):22246–53.
- [26] Xing M, et al. Association between BRAF V600E mutation and mortality in patients with papillary thyroid cancer. *JAMA* 2013;309(14):1493–501.
- [27] Zoghbi A, et al. BRAF mutation in papillary thyroid carcinoma: predictive value for long-term prognosis and radioiodine sensitivity. *Eur Ann Otorhinolaryngol, Head Neck Dis* 2014;131(1):7–13.
- [28] Al-Masri M, et al. BRAF V600E mutation in papillary thyroid carcinoma: its relation to clinical features and oncologic outcomes in a single cancer centre experience. *Endocr Connect* 2021;10(12):1531–7.
- [29] Gawel AM, et al. Analysis of the role of FRMD5 in the biology of papillary thyroid carcinoma. *Int J Mol Sci* 2021;22:13.
- [30] Schindelin J, et al. Fiji: an open-source platform for biological-image analysis. *Nat Methods* 2012;9(7):676–82.
- [31] Love MI, Huber W, Anders S. Moderated estimation of fold change and dispersion for RNA-seq data with DESeq2. *Genome Biol* 2014;15(12):550.

- [32] Ashburner M, et al. Gene ontology: tool for the unification of biology. The Gene Ontology Consortium. *Nat Genet* 2000;25(1):25–9.
- [33] Gillespie M, et al. The reactome pathway knowledgebase 2022. *Nucleic Acids Res* 2021;50(D1). D687–D692.
- [34] Ulgen E, Ozisik O, Sezerman OU. pathfindR: An R Package for Comprehensive Identification of Enriched Pathways in Omics Data Through Active Subnetworks. *Front Genet* 2019;10:858.
- [35] Chen H, Boutros PC. VennDiagram: a package for the generation of highly-customizable Venn and Euler diagrams in R. *BMC Bioinforma* 2011;12:35.
- [36] Team, R.C., *R: A language and environment for statistical computing*. R Foundation for Statistical Computing. 2014.
- [37] Hadley, W., *ggplot2: Elegant Graphics for Data Analysis*. 2016.
- [38] Gujral TS, et al. A novel RET kinase- $\beta$ -catenin signaling pathway contributes to tumorigenesis in thyroid carcinoma. *Cancer Res* 2008;68(5):1338–46.
- [39] Müller T, et al. Regulation of epithelial cell migration and tumor formation by  $\beta$ -catenin signaling. *Exp Cell Res* 2002;280(1):119–33.
- [40] Fukuda T, Kiuchi K, Takahashi M. Novel mechanism of regulation of rac activity and lamellipodia formation by RET tyrosine kinase\*. *J Biol Chem* 2002;277(21):19114–21.
- [41] Wan PT, et al. Mechanism of activation of the RAF-ERK signaling pathway by oncogenic mutations of B-RAF. *Cell* 2004;116(6):855–67.
- [42] Deng Z, et al. Radiation-induced c-jun activation depends on MEK1-ERK1/2 signaling pathway in microglial cells. *PLOS ONE* 2012;7(5):e36739.
- [43] Ouwens DM, et al. Growth factors can activate ATF2 via a two-step mechanism: phosphorylation of Thr71 through the Ras-MEK-ERK pathway and of Thr69 through RalGDS-Src-p38. *EMBO J* 2002;21(14):3782–93.
- [44] Gupta P, Prywes R. ATF1 phosphorylation by the ERK MAPK pathway is required for epidermal growth factor-induced c-jun expression\*. *J Biol Chem* 2002;277(52):50550–6.
- [45] Clarke N, et al. Epidermal growth factor induction of the c-jun promoter by a rac pathway. *Mol Cell Biol* 1998;18(2):1065–73.
- [46] De Cesare D, et al. Rsk-2 activity is necessary for epidermal growth factor-induced phosphorylation of CREB protein and transcription of c-fos gene. *Proc Natl Acad Sci USA* 1998;95(21):12202–7.
- [47] Gille H, et al. ERK phosphorylation potentiates Elk-1-mediated ternary complex formation and transactivation. *Embo J* 1995;14(5):951–62.
- [48] Shore P, Sharrocks AD. The transcription factors Elk-1 and serum response factor interact by direct protein-protein contacts mediated by a short region of Elk-1. *Mol Cell Biol* 1994;14(5):3283–91.
- [49] Kasza A, et al. The ETS domain transcription factor Elk-1 regulates the expression of its partner protein, SRF\*. *J Biol Chem* 2005;280(2):1149–55.
- [50] Bruning JC, et al. Ribosomal subunit kinase-2 is required for growth factor-stimulated transcription of the c-Fos gene. *Proc Natl Acad Sci USA* 2000;97(6):2462–7.
- [51] Langfermann DS, Rössler OG, Thiel G. Stimulation of B-Raf increases c-Jun and c-Fos expression and upregulates AP-1-regulated gene transcription in insulinoma cells. *Mol Cell Endocrinol* 2018;472:126–39.
- [52] Marinissen MJ, et al. The small GTP-binding protein RhoA regulates c-Jun by a ROCK-JNK signaling axis. *Mol Cell* 2004;14(1):29–41.
- [53] Parri M, Chiarugi P. Rac and Rho GTPases in cancer cell motility control. *Cell Commun Signal* 2010;8:23.
- [54] Clerk A, Sugden PH. Small guanine nucleotide-binding proteins and myocardial hypertrophy. *Circ Res* 2000;86(10):1019–23.
- [55] Ward LSC, et al. Podoplanin regulates the migration of mesenchymal stromal cells and their interaction with platelets. *J Cell Sci* 2019;132:5.
- [56] Lin MN, et al. Involvement of PI3K and ROCK signaling pathways in migration of bone marrow-derived mesenchymal stem cells through human brain microvascular endothelial cell monolayers. *Brain Res* 2013;1513:1–8.
- [57] Bos JL, Rehmann H, Wittinghofer A. GEFs and GAPs: critical elements in the control of small G proteins. *Cell* 2007;129(5):865–77.
- [58] Stanley, R.J. and G.M. Thomas, *Activation of G Proteins by Guanine Nucleotide Exchange Factors Relies on GTPase Activity*. (1932–6203 (Electronic)).
- [59] He H, et al. The roles of GTPase-activating proteins in regulated cell death and tumor immunity. *J Hematol Oncol* 2021;14(1):171.
- [60] Welch HC, et al. P-Rex1, a PtdIns(3,4,5)P<sub>3</sub>- and Gbetagamma-regulated guanine-nucleotide exchange factor for Rac. *Cell* 2002;108(6):809–21.
- [61] Welch HCE. Regulation and function of P-Rex family Rac-GEFs. *Small GTPases* 2015;6(2):49–70.
- [62] Zhou S, et al. The mTOR-RUNX1 pathway regulates DC-SIGN expression in renal tubular epithelial cells. *Biochem Biophys Res Commun* 2019;519(3):620–5.
- [63] Angela M, et al. Fatty acid metabolic reprogramming via mTOR-mediated inductions of PPAR $\gamma$  directs early activation of T cells. *Nat Commun* 2016;7(1):13683.
- [64] Tabatabaieian H, et al. The emerging roles of WBP2 oncogene in human cancers. *Oncogene* 2020;39(24):4621–35.
- [65] Zhou S, et al. The mTOR-RUNX1 pathway regulates DC-SIGN expression in renal tubular epithelial cells. *Biochem Biophys Res Commun* 2019;519(3):620–5.
- [66] Cozzolino M, et al. p120 Catenin is required for growth factor-dependent cell motility and scattering in epithelial cells. *Mol Biol Cell* 2003;14(5):1964–77.
- [67] Polisenio L, et al. A coding-independent function of gene and pseudogene mRNAs regulates tumour biology. *Nature* 2010;465(7301):1033–8.
- [68] Xue, P., et al., *Up-regulation of PTEN via LPS/AP-1/NF- $\kappa$ B pathway inhibits trophoblast invasion contributing to preeclampsia*. (1872–9142 (Electronic)).
- [69] Wang L, Lv Y, Liu G. The roles of SHANK1 in the development of colon cancer. *Cell Biochem Funct* 2020;38(5):669–75.
- [70] Zandy NL, Pendergast AM. Abl tyrosine kinases modulate cadherin-dependent adhesion upstream and downstream of Rho family GTPases. *Cell Cycle* 2008;7(4):444–8.
- [71] Tong H, et al. c-Abl tyrosine kinase regulates neutrophil crawling behavior under fluid shear stress via Rac/PAK/LIMK/cofilin signaling axis. *J Cell Biochem* 2018;119(3):2806–17.
- [72] Servitja, J.M., et al., *Rac1 function is required for Src-induced transformation. Evidence of a role for Tiam1 and Vav2 in Rac activation by Src*. (0021–9258 (Print)).
- [73] Zhu EY, et al. SRC-RAC1 signaling drives drug resistance to BRAF inhibition in dedifferentiated cutaneous melanomas. *npj Precis Oncol* 2022;6(1):74.